GA-3396

40-MW(E) PROTOTYPE HIGH-TEMPERATURE GAS-COOLED REACTOR

Quarterly Progress Report for the Period Ending June 30, 1962

June 30, 1963
[DTI Issuance Date]

General Atomic Division
General Dynamics Corporation
San Diego, California

UNITED STATES ATOMIC ENERGY COMMISSION • DIVISION OF TECHNICAL INFORMATION

DISCLAIMER

LEGAL NOTICE

Printed in USA. Price $1.50. Available from the Office of Technical Services, Department of Commerce, Washington 25, D. C.

USAEC Division of Technical Information Extension, Oak Ridge, Tennessee

GENERAL ATOMIC

DIVISION OF

GENERAL DYNAMICS

JOHN JAY HOPKINS LABORATORY FOR PURE AND APPLIED SCIENCE

P.O. BOX 608. SAN DIEGO 12. CALIFORNIA

GA-3396

REACTOR TECHNOLOGY

40-MW(E) PROTOTYPE HIGH-TEMPERATURE GAS-COOLED REACTOR RESEARCH AND DEVELOPMENT PROGRAM

QUARTERLY PROGRESS REPORT FOR THE PERIOD ENDING JUNE 30, 1962

Contract AT(04-3)-314

U. S. Atomic Energy Commission

HTGR QUARTERLY REPORT SERIES

GA-1235—October, November, December, 1959
(including a summary of work between January 1, 1959, and September 30,1959)

GA-1378—January, February, March, 1960

GA-1640—April, May, June, 1960

GA-1774—July, August, September, 1960

GA-1982—October, November, December, 1960

GA-2204—January, February, March, 1961

GA-2493—April, May, June, 1961

GA-2747—July, August, September, 1961

GA-2861—October, November, December, 1961

GA-3132—January, February, March, 1962

SUMMARY

This report covers the work performed by General Atomic Division of General Dynamics Corporation under U. S. Atomic Energy Commission Contract AT(04-3)-314 during the period from April 1, 1962, through June 30, 1962. This contract calls for research and development specifically directed toward the construction of a 40-Mw(e) prototype power plant employing a high-temperature, gas-cooled, graphite-moderated reactor known as the HTGR.

The more important developments in the HTGR program during this period are briefly summarized below. These subjects are treated in more detail in the body of the report.

Irradiation of element III-B in the in-pile loop continued satisfactorily during the quarter. As the quarter ended, the element had generated a total of 136.3 Mw-hr of fission heat. The gross activity in the purge stream increased slightly to about 350 $\mu c/cm^3$. By taking larger gas samples than were previously taken, a value of 0.02 $\mu c/cm^3$ was obtained for the gross activity of the primary loop.

Element III-A, which was removed from the loop last quarter after generating 133 Mw-hr of fission heat, was disassembled and examined. No fuel-compact damage of any type was visible. Determination of the distribution of fission products in the element is under way. To date, only preliminary results are available.

Fission-product-release data for in-pile-loop element III-A were calculated during the quarter. During the 133 Mw-hr of operation, the release fraction increased by approximately one order of magnitude. Also calculated were the xenon and krypton release data for the first 100 Mw-hr of III-B operation. The release rate for the longer-lived isotopes increased by about a factor of 10 and that of the shorter-lived isotopes by about a factor of 100.

A test was run in which the in-pile-loop purge flow was stopped. The primary-loop activity level rose sharply during the first hour, increased at a slower rate for the next 11 hr, and then appeared to level off. When purge flow was resumed, the gross activity in the primary loop was cleaned up with a half life of about 2.2 hr.

An attempt was made to identify Cs^{137} and Ba^{140} plateout in portions of the in-pile loop. A very small amount of cesium (less than a monolayer) was found, but no barium could be detected.

The validity of two basic assumptions made in the one-dimensional burnup code FEVER was investigated this quarter. The first assumption is that the microscopic four-group constants do not change with exposure. The effect of group cross-section changes through life has been determined by re-evaluating the fine-group spectra after each 300 days of exposure. It was found that the spectrum within each broad group had significantly softened after each 300-day period. The effect of allowing the fine-group spectra to vary is to increase the reactivity at all times during life, resulting in a 10% extension of the reactivity life of the core.

The other assumption involves the homogenization of the core in the axial direction and representation of leakage by means of a buckling term. The effect of this assumption was investigated by comparing FEVER calculations with two-dimensional DDB calculations in RZ geometry. The DDB results gave a higher reactivity at the beginning of life and a lower reactivity at the end of life. Most of the difference in the end-of-life value is a consequence of increased burnout of fuel in regions of higher importance.

As a result of extensive lifetime studies and power-distribution and temperature-coefficient calculations, the initial fuel loading for the Peach Bottom core has been specified. A series of control-rod-worth calculations and a recalculation of the postulated rod-fall accident have been made for this loading.

The test of the prototype control rod and drive was satisfactorily completed during the quarter. During the course of the test the drive completed 590,641 starts and stops, 5,756 scrams, and more than 2.6 million inches of random regulating motion in helium at reactor temperatures. These totals far exceed the expected life requirements of the system.

Preparations are being made for testing the prototype emergency shutdown rod and drive.

The apparatus for the barium permeation experiment with a full-diameter sleeve was completed, and preliminary calibration runs were started. Following these runs, the system will be operated until an equilibrium distribution of barium has been reached. At that time, a series of corings will be made on all of the compacts and the sleeve to evaluate the over-all barium and strontium distribution.

Other experiments on barium behavior, including permeation experiments with reduced-scale fuel elements and experiments on the vaporization,

sorption, and diffusion of barium, were continued, and the data are being analyzed.

Measurements were made to compare the room-temperature back diffusion of argon, krypton, and xenon through a sample of sleeve graphite against a helium pressure difference. The results show that the difference between the effective back-diffusion coefficients of krypton and xenon seems to increase with increasing helium pressure difference across the sleeve. The argon and krypton back-diffusion data at an average pressure of 3 atm are essentially the same.

A FORTRAN code has been written to recalculate the retention of neutron poison material and fission products in the core as well as their condensation on and revaporization from the upper reflector following a complete loss-of-coolant-circulation accident.

THIS PAGE

WAS INTENTIONALLY

LEFT BLANK

CONTENTS

TASK VIII

APPENDIXES

Figures

TASK I. DEVELOPMENT OF MATERIALS FOR REACTOR CORE

1. 1. GRAPHITE SLEEVE MATERIAL

The series of physical- and mechanical-property determinations on graphite sleeve materials was continued during the quarter. Table 1. 1 presents the data obtained to date, including those reported in the previous quarterly report. Also included in Table 1. 1 are some data obtained on two graphites, R-1 and HLM-85 base stock, which are candidates for fuel-element parts other than sleeves.

1. 2. IRRADIATION TESTING

Capsule Irradiation

The irradiation of capsules GA-311-10 and -11, which contain graphite samples, is continuing. These capsules will be discharged near the end of the year.

Two irradiation capsules designed to evaluate the behavior of 30 wt-% boron as B_4C in an extruded-graphite-tube geometry are being fabricated. The capsules will be exposed to temperatures of approximately 700°F, one for two cycles and one for six cycles. The capsules will contain B_4C–graphite material from three different suppliers.

In-pile-loop Program

Operation of the in-pile loop continued to be satisfactory during the quarter. As the quarter ended, element III-B had generated a total of 136. 3 Mw-hr of fission heat. This is equivalent to the exposure element III-A had received when it was discharged from the reactor. Maximum temperatures of 2750°F in the fuel and 1300°F in the exit gas were observed during periods of high power generation (to 82 kw). The fractional release of fission-product gases as observed in the purge stream increased slightly during the quarter. The maximum gross activity in the purge stream was approximately 350 $\mu c/cm^3$. The main-loop gross activity was approximately 0. 02 $\mu c/cm^3$ as determined from 600 cm^3 samples (the normal 2. 7 cm^3 sample contains insufficient activity against the general reactor background).

Table 1.1

MECHANICAL AND PHYSICAL PROPERTIES OF VARIOUS GRAPHITES

Sample	Tensile Strength at RT (psi)	Hoop Strength (psi)	Modulus of Rupture at 2700°F (psi)		Shear (psi)		Modulus of Elasticity at 2700°F (10^6 psi)		Thermal Conductivity at 2700°F (Btu/ft-hr-°F)	Density (g/cm^3)	Coefficient of Thermal Expansion at 1832°F (10^{-6} in./in.-°F)	
			∥	⊥	∥	⊥	∥	⊥			∥	⊥
GL1-S-12			5470	5610			0.940	0.872		1.814		
			5350	5840			0.785	1.275		1.849		
GL1-S-16	2450	1600	6030	3680	2850	2150	1.310	0.924	18.8	1.869		
	2850		5340	3130	2950	2500	1.081	1.175		1.865		
GL1-S-18	1700	1850	6060	4700	3100	2750	1.018	0.740	19	1.910	1.2	2.2
										1.909		
GL1-S-19	1680											
	1820											
GL1-S-21	2800		8000	5570	3750	3150	1.503	0.992	24	1.930		
	3600		7400	5900	3750	3250	1.543	0.968		1.934		
GL1-S-22	2900		7710	5140			1.380	0.905		1.822		
	3360		8210	5160			1.421	0.775				
NC1-S-11	3100		5230	5750			0.942	0.848				
	3650		4540				1.050					
R-1	1200		4750	5000	1800	1775				1.66		
	1900											
HLM-85 (base stock)	1800						0.80	0.71	20.5	1.80		

∥ —Parallel to the extrusion axis.

⊥ —Perpendicular to the extrusion axis.

A zero-purge-flow test was conducted over a 24-hr period, and an attempt was made to identify cesium and barium plateout in the loop. Details of both these investigations are reported in Task VI.

A main-loop valve, AV-2, which had a leaking bellows was removed with difficulty. Peach Bottom design engineers and a Bechtel representative were present during the valve removal to inspect the work area for possible Peach Bottom applications. Loop leakage has been extremely low since the source of leakage was found and repaired.

Postirradiation Examination. During the quarter, in-pile-loop element III-A was received at the General Atomic hot cell. Disassembly was hampered somewhat by the penetration of the resin compound (introduced in the element after completion of irradiation) into the trap and compact slots. The sleeve had to be cut open in order to remove some of the internal parts. The internal trap was opened and two slots were exposed for examination and sampling. Samples taken from various locations in the trap are being analyzed.

Five fuel compacts were examined, measured, and photographed. No damage of any type was visible; the compacts' appearance was comparable to their appearance before irradiation. Figure 1.1 shows an unirradiated fuel compact (on the left) and a compact which was removed from the hot zone of element III-A after irradiation (on the right).

Permeability tests were made on four jointed samples which were removed from the III-A test element. The results, which are listed in Table 1.2, show that no significant changes occurred as a result of irradiation. No other physical changes were observed.

Fuel-element Fabrication for In-pile Loop. Fuel compacts containing carbon-coated (fully enriched U-Th)C_2 particles and Rh_2O_3 powder were fabricated for test element III-C by warm-pressing in the Stellite 6B die. Most of the compacts developed radial hairline cracks upon ejection from the die. The cracks caused no damage to the carbides, since no hydrolysis was observed in the cracked areas even when a representative compact was immersed in water for several weeks.

A 3-in.-thick end plug was silicon-brazed to sleeve GLI-S-17, and the permeabilities of the components measured prior to joining were the same as that of the assembly after brazing. After insertion of the internal components into the element, a tapered HLM-85 plug was cemented (using C-6) to the top of the element. The cemented joint was cured and then carbonized to 650°C in the vacuum-brazing and vacuum-outgassing furnace.

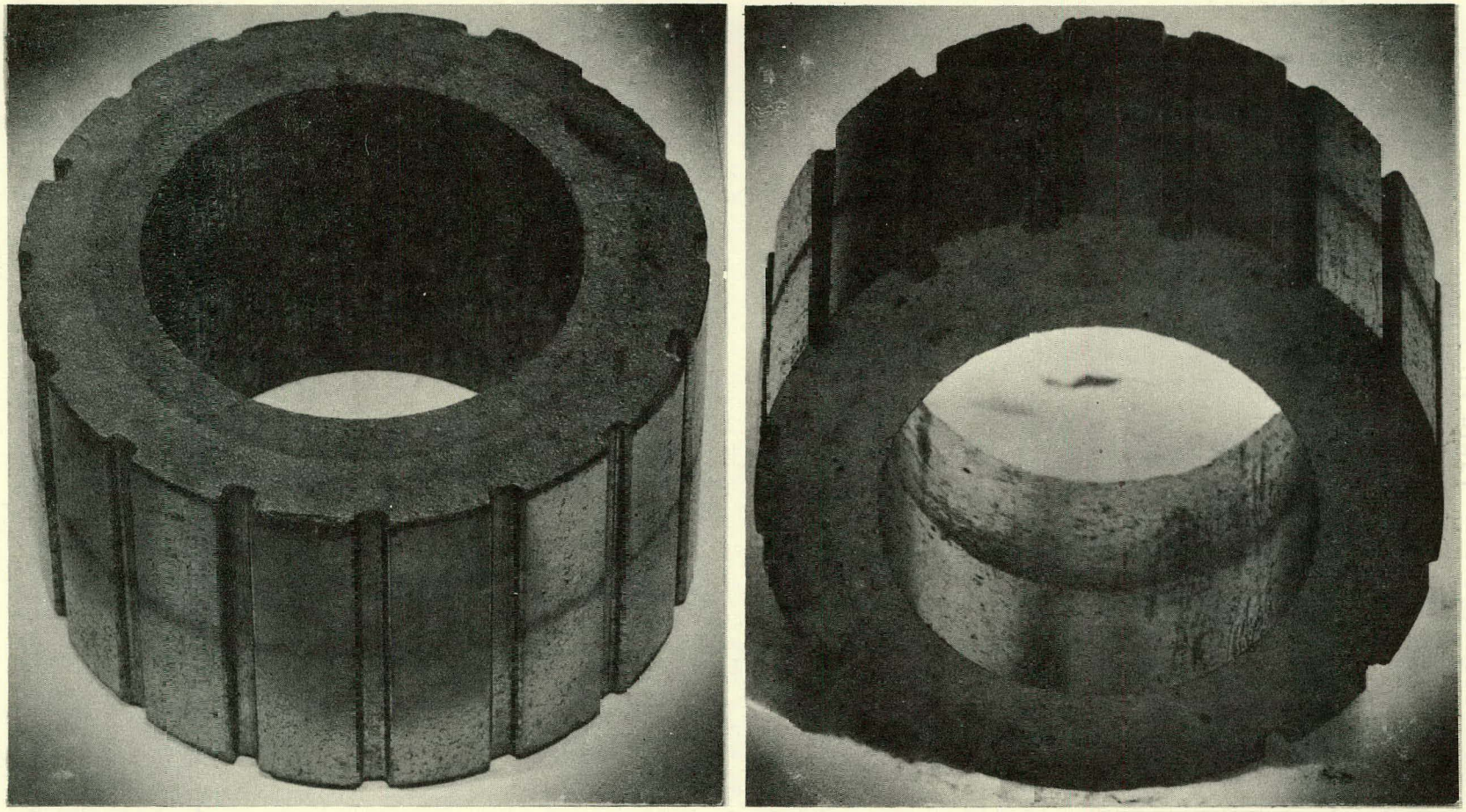

Fig. 1. 1--Unirradiated fuel compact (left); compact removed from hot zone of element III-A after irradiation (right)

Table 1.2

PERMEABILITY OF JOINTED GRAPHITE SAMPLES BEFORE AND AFTER IRRADIATION

Specimen	Type of Graphite	Joint Material	Permeability Before III-A Test	Permeability After III-A Test
GLC-2	Great Lakes impregnated tube; GA impregnated EYX 60 disk	Silicon	2.44×10^{-5}	8×10^{-5}
GLC-8	Great Lakes impregnated tube; GA impregnated EYX 60 disk	Silicon	2.45×10^{-4}	1.3×10^{-4}
GL-6	Great Lakes impregnated	$MoSi_2$	4.67×10^{-2}	5.4×10^{-2}
GL-E-1	Great Lakes impregnated	C-6	4.36×10^{-3}	1.3×10^{-2}

1.3. CHEMISTRY EXPERIMENTS SUPPORTING MATERIALS DEVELOPMENT

Reaction of Nitrogen with UC_2

The thermodynamics of the various possible reactions of N_2 with UC_2 have been investigated to determine the feasibility of using nitrogen as a carrier gas in the fuel-particle coating process.

The reactions studied were:

$$UC_2(s) + 1/2\ N_2(g) = UN(s) + 2C(s)\ , \qquad (1)$$

$$UC_2(s) + 3/2\ N_2(g) = UN(s) + C_2N_2(g)\ , \qquad (2)$$

$$UC_2(s) + 3/2\ N_2(g) = UN(s) + 2CN(g)\ , \qquad (3)$$

$$UC_2(s) + 3/2\ N_2(g) + H_2(g) = UN(s) + 2HCN(g)\ . \qquad (4)$$

Since the gaseous reaction products of the last three reactions are all formed from the elements highly endothermically, it is clear that they will

constitute a negligible contribution to the nitride formation at even moderately elevated temperatures. The only important reaction is reaction (1).* The equilibrium pressures of nitrogen at temperatures below 2000°K are less than 1 atm. This means that maintaining a nitrogen pressure of 1 atm in the coating apparatus would convert the carbide to nitride. The equilibrium pressures of N_2 for reaction (1) are given in Table 1.3. A nitrogen pressure greater than these values will tend to drive reaction (1) to the right; lower nitrogen pressures will result in conversion of the nitride to the carbide.

Table 1.3

URANIUM CARBIDE–URANIUM NITRIDE EQUILIBRIA FOR THE REACTION $UC_2(s) + 1/2\ N_2(g) = UN(s) + 2C(s)$

Temp. (°K)	ΔF^o_T	K_1	P_{N_2} (atm)
298	-34.6	2.3×10^{25}	2.1×10^{-13}
1000	-20.8	3.5×10^{4}	5.4×10^{-3}
1200	-16.9	1.2×10^{3}	2.9×10^{-2}
1400	-12.9	1.0×10^{2}	9.8×10^{-2}
1600	-9.0	17	0.24
1800	-5.0	4.1	0.49
2000	-1.1	1.3	0.88

These calculations have been carried out using pure UC_2 as the carbide species, since the thermodynamic data on uranium compounds are more readily available and more reliable than the data on thorium. However, the species to be used in the Peach Bottom reactor is 7 ThC_2:1 UC_2. An examination of the few crude estimates for ThC_2 and Th_3N_4 indicates that, if the estimates are reliable, the situation will be still more unfavorable for thorium, i.e., more nitride formation can be expected.

From the above, it can be concluded, assuming that reaction kinetics are unfavorable (i.e., that reaction (1) is relatively fast), that it will not be possible to use nitrogen as a carrier gas until the particles have at least a thin, impermeable carbon coating.

In estimating the amounts of gaseous carbon–nitrogen compounds in the effluent stream, it is clear that the maximum amounts that can be expected will not result from reactions (2) to (4), but will come from the formation reactions from the elements, since in these reactions carbon is

*The only nitride which must be considered is UN. The dinitride and sesquinitride are both unstable with respect to UN at elevated temperatures.

in a state of unit activity. These formation reactions and their equilibrium constants are:

$$2C(s) + N_2(g) = C_2N_2(g), \qquad K_5 = \frac{P_{C_2N_2}}{P_{N_2}}, \tag{5}$$

$$C(s) + 1/2\ N_2(g) = CN(g), \qquad K_6 = \frac{P_{CN}}{P_{N_2}^{1/2}}, \tag{6}$$

$$C(s) + 1/2\ N_2(g) + 1/2\ H_2(g) = HCN, \qquad K_7 = \frac{P_{HCN}}{P_{N_2}^{1/2}\ P_{H_2}^{1/2}}. \tag{7}$$

The equilibrium constants and partial pressures of the product gases are given in Table 1.4 for an assumed nitrogen pressure of 1 atm and hydrogen pressure of 0.2 atm (based on complete dissociation of 0.1 atm of CH_4). The only product gas of significance will be HCN, and its partial pressure in a 1400°C effluent stream should be less than 5 mm Hg (1 mm Hg = 1.3×10^{-3} atm). Thus, cleanup of the off-gas stream should not be difficult.

Table 1.4

GASEOUS EQUILIBRIA OF CARBON–NITROGEN COMPOUNDS[a]

	Reaction (5)[b]	Reaction (6)[b]	Reaction (7)[b]		
Temp. (°K)	$K_5 = P_{C_2N_2}$ (atm)	$K_6 = P_{CN}$ (atm)	K_7	$P_{H_2}^{1/2}$	P_{HCN} (atm)
298	7.4×10^{-53}	2.7×10^{-62}	9.1×10^{-22}	4.5×10^{-1}	4.1×10^{-22}
1000	1.1×10^{-14}	2.5×10^{-15}	9.1×10^{-6}	4.5×10^{-1}	4.1×10^{-6}
1200	6.0×10^{-12}	5.0×10^{-12}	1.2×10^{-4}	4.5×10^{-1}	5.4×10^{-5}
1400	5.2×10^{-10}	1.1×10^{-9}	7.6×10^{-4}	4.5×10^{-1}	3.4×10^{-4}
1600	1.5×10^{-8}	6.8×10^{-8}	3.0×10^{-3}	4.5×10^{-1}	1.4×10^{-3}
1800	2.0×10^{-7}	1.5×10^{-6}	8.7×10^{-3}	4.5×10^{-1}	3.9×10^{-3}
2000	1.6×10^{-6}	1.9×10^{-5}	2.0×10^{-2}	4.5×10^{-1}	9.0×10^{-3}

[a]From Dow Chemical Company, Thermal Laboratory, JANAF Interim Thermochemical Tables, Vol. 1, Midland, Michigan, December 31, 1960.

[b]Assuming a hydrogen pressure of 0.2 atm and a nitrogen pressure of 1.0 atm.

If the use of nitrogen is sufficiently attractive, experiments will be required to check the kinetics of reaction (1) and/or to determine if thin, impermeable carbon coatings can be readily produced.

Catalytic Effect of Barium and Strontium

Strontium and barium when sorbed by graphite are known to catalyze the steam–graphite reaction. Previous work described in the last quarterly report showed that when 0.04 wt-% barium or strontium is impregnated in graphite-matrix compact material, the steam–graphite reaction rate is increased by a factor of 1.6 in the temperature range 855° to 1050°C, under conditions of 3.3% steam in helium flowing at 110 ml/min.

Some recent work has shown that increasing the flow rate by a factor of ten decreases somewhat the catalytic effect of the sorbed metals. Table 1.5 lists the results of the higher-flow test along with the results of the original test for comparison purposes. One might conclude from these data that the reaction is at least partially diffusion controlled and that by increasing the gas velocity (approaching turbulent conditions) the catalytic effect may be reduced still further.

Table 1.5

CATALYTIC EFFECT OF BARIUM AND STRONTIUM ON THE STEAM–GRAPHITE REACTION

Sample	Flow Rate (ml/min)	Reaction Rate (%/hr)	Catalytic Ratio
0.04% Ba	110	0.889	1.69
0.02% Ba	110	0.875	1.66
0.01% Ba	110	0.621	1.18
0.04% Sr	110	0.863	1.64
0.02% Sr	110	0.646	1.23
0.01% Sr	110	0.554	1.06
Control	110	0.525	1.0
0.04% Ba	1030	4.9	1.37
0.02% Ba	1030	3.7	1.03
0.01% Ba	1030	3.6	1.0
0.04% Sr	1030	3.1	0.86
0.02% Sr	1030	3.2	0.89
0.01% Sr	1030	2.8	0.78
Control	1030	3.6	1.0

More important, perhaps, in terms of oxidation of the reactor core is the catalytic effect of barium or strontium on sleeve graphite. Accordingly, some experimentation has been carried out using barium-impregnated HLM-85 specimens. These samples were loaded with barium by exposure to a Ba^{133}-tagged BaO–graphite powder mixture at 1000°C. It was found that barium vapor, arising from the reaction BaO + C = CO + Ba, soaks into the graphite fairly uniformly at 1000°C, providing that sufficient time is allowed (~10 hr). The barium concentration in each specimen is determined by ordinary radio-counting techniques.

The results of the steam–graphite experiments on barium-soaked HLM-85 graphite are shown in Fig. 1.2. These specimens were exposed to 3.3% steam in helium flowing at 1 liter/min.

One run in which very high barium loadings were used (not shown in the figure) yielded somewhat surprising results. Samples with 2.6% barium averaged 5.6% weight loss per hour for 15.5 hr. Samples with 2.9% barium were completely gasified in 15.5 hr. (A reaction rate in excess of 6.4%/hr would account for 100% weight loss.) It appears that increasing the barium content over 0.05% does not appreciably increase the oxidation rate.

Work by members of the Dragon Project in Norway has shown that silica may poison the catalysis by barium. Since our experiments were performed in a quartz system, the experimental data gleaned thus far may be somewhat in error. Steps are presently being taken to preclude the possibility of contamination by silica in some additional experiments.

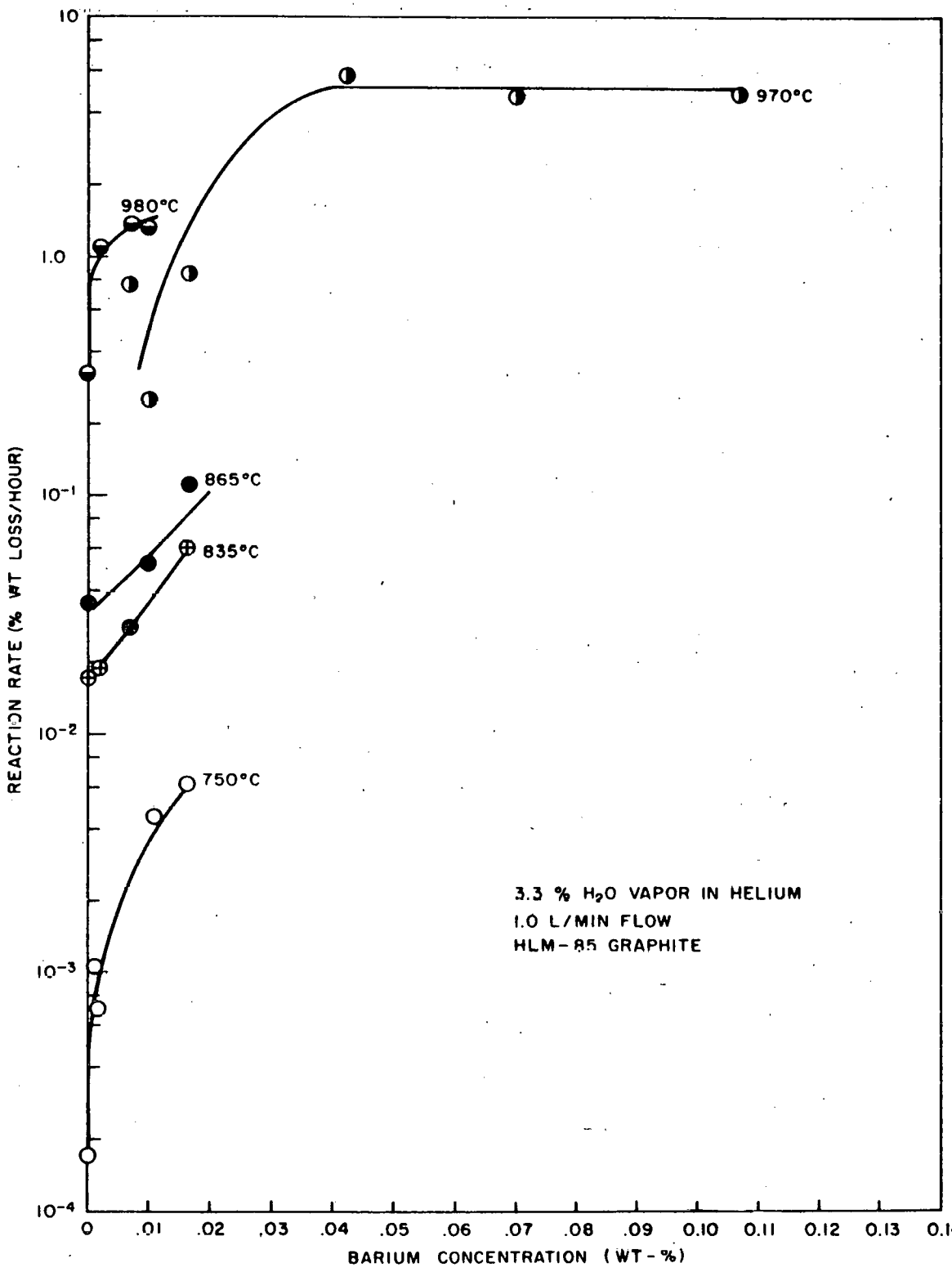

Fig. 1.2--Catalysis of the steam–graphite reaction by sorbed barium

TASK II. DEVELOPMENT OF REACTOR CORE AND REFLECTOR

2. 1. NUCLEAR DESIGN AND THEORETICAL PHYSICS

Lifetime Studies

Most of the previously reported lifetime studies have been performed using the one-dimensional burnup code, FEVER. Two basic assumptions are made in the FEVER program; the validity of these assumptions was investigated during this quarter. First, it is assumed in the program that the microscopic four-group constants do not change with exposure. Since only one thermal group can be used, this means that the time dependence of the thermal-neutron spectrum is not taken into account. Second, only the radial dimension is treated explicitly. In the axial direction, the core has to be homogenized, and leakage has to be represented by means of a buckling term.

The effect of group cross-section changes through life has been determined for a typical core loading. This was accomplished by re-evaluating the fine-group spectra after 300, 600, and 900 days of exposure. The cross sections appropriate to the beginning of each of these 300-day steps were obtained by use of the GAM and GATHER codes in conjunction with the appropriate atom densities as predicted by the FEVER depletion code, and these cross sections were assumed to be invariant during the subsequent 300-day exposure.

After each 300 days of depletion, it was found that the spectrum within each broad group had significantly softened. The effect of this spectral softening upon the reactivity of the system can be seen from Fig. 2. 1. The reactivity is increased at all times during life when the fine-group spectra are allowed to vary, which results in a 10% extension of the reactivity life of the core.

The effect of the axial dimension on the lifetime characteristics has been studied by comparing FEVER calculations with two-dimensional DDB calculations in RZ geometry. The DDB program has been checked out carefully. It was found to agree very closely with FEVER for mocked-up zero- or one-dimensional problems.

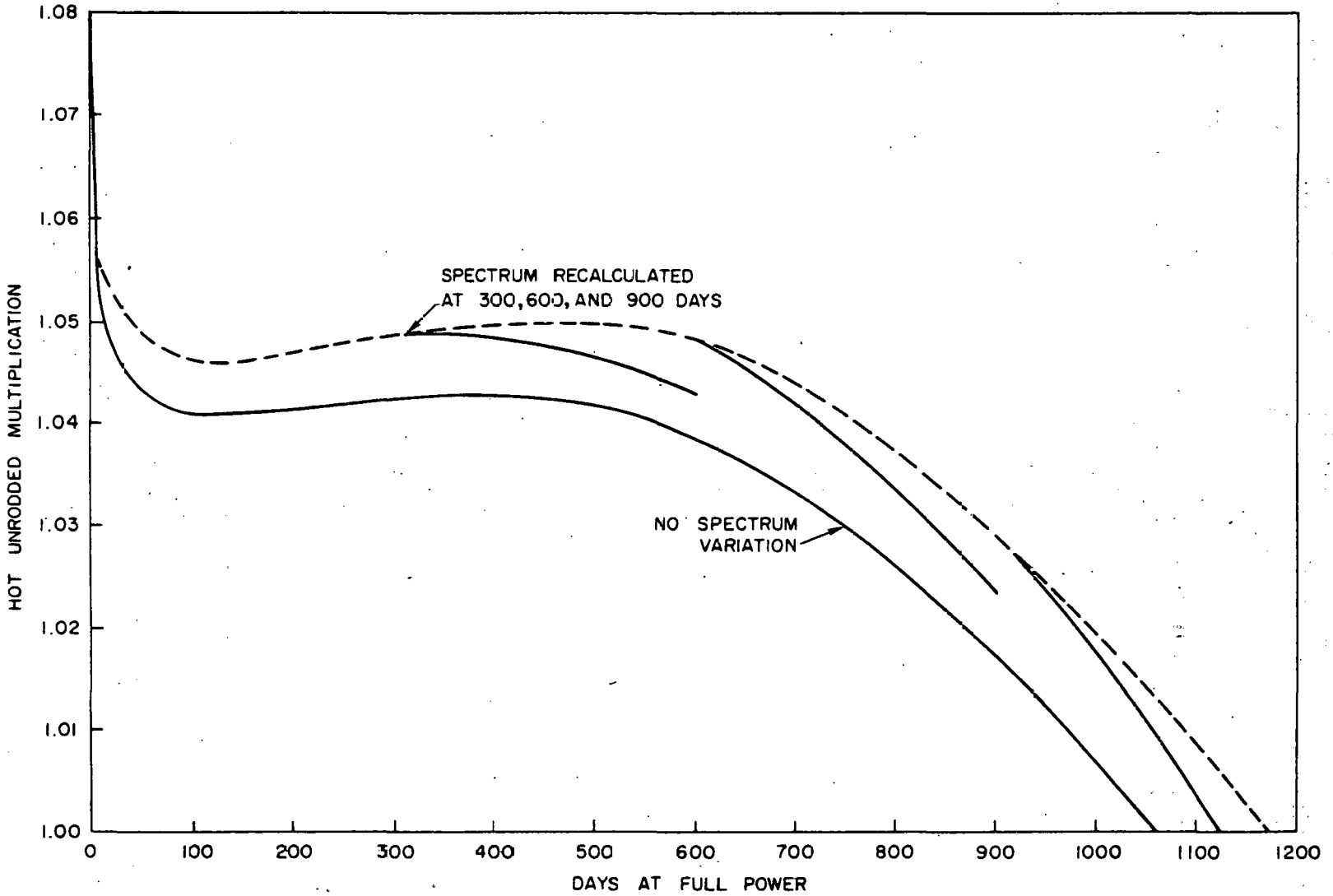

Fig. 2.1--Effect on hot, unrodded multiplication of allowing the fine-group spectra to vary with exposure

Identical one-dimensional FEVER and two-dimensional DDB calculations were performed for a typical core loading. The hot unrodded multiplication as a function of time at full power is given for the one- and two-dimensional calculations in Fig. 2.2. The beginning-of-life reactivity from the two-dimensional calculation is 0.009 $\Delta\rho$ higher than the value from the one-dimensional calculation. The reduction in the total leakage accounts for 0.003 $\Delta\rho$.

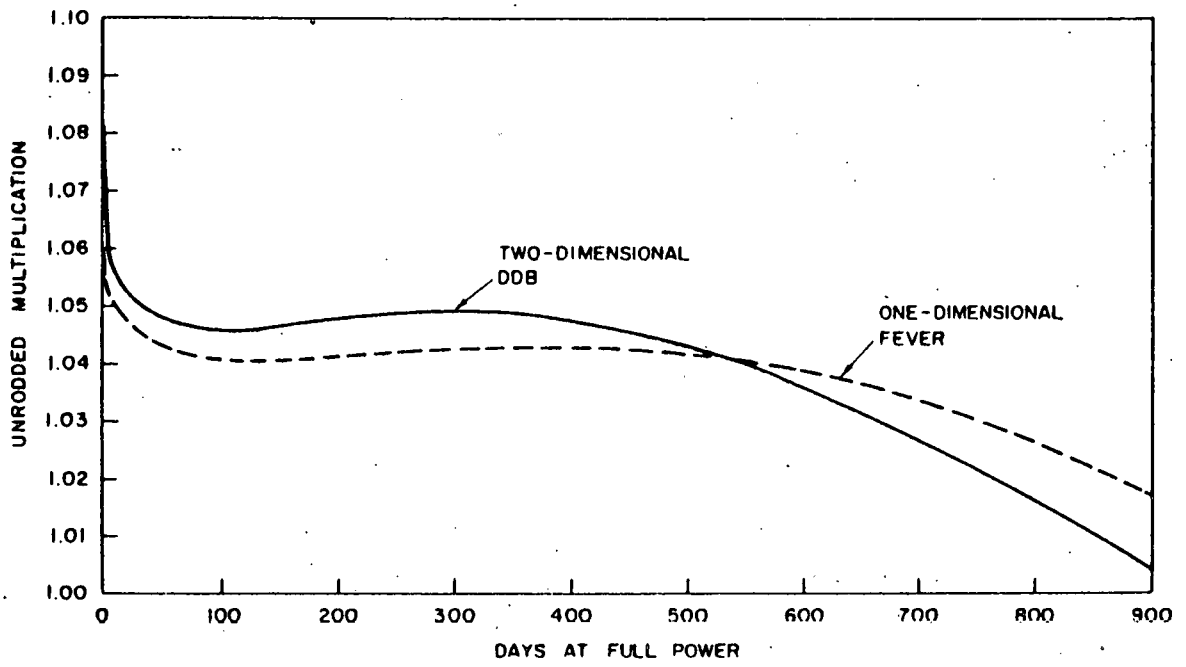

Fig. 2.2--Comparison of one- and two-dimensional burnup calculations

After 900 days of burnup, the two-dimensional calculation is 0.013 $\Delta\rho$ lower than the one-dimensional calculation. The differences in the 900-day loading between the two-dimensional and one-dimensional calculation are very small, and the increased burnout of fuel in two dimensions can account for a decrease in reactivity of only about 0.009 $\Delta\rho$ over the one-dimensional calculation. Therefore, most of the difference in the excess reactivity at 900 days is a consequence of increase burnout of fuel in the regions of higher importance.

Fuel-loading Specification

The extensive lifetime studies and power-distribution and temperature-coefficient calculations resulted in the following specification for the initial fuel loading:

Th^{232}	1,652.2 kg
U^{235}	220.0 kg
U^{238}	16.05 kg
Rh^{103}	8.0 kg
Carbon	21,331 kg
Boron	1.10 kg

A graph of hot excess and cold shutdown reactivity through life for this loading is given in Fig. 2.3, and the over-all and prompt temperature coefficients for the end-of-life condition are shown in Fig. 2.4. Power distributions for beginning and end of life are shown in Figs. 2.5 and 2.6, in which radial and axial power plots are combined to form three-dimensional surfaces. The power peak at the core–reflector interface is underestimated, since only one thermal group was used in obtaining these power distributions. Multithermal-group calculations indicate that the power peak remains at the center of the core. As a result of preferential fuel burnout, the local peak at the interface decreases with exposure.

Control-rod Worth

A series of control-rod-worth calculations for the specified core loading was done in XY geometry with the GAMBLE code. The method of representing the control rods has been described in a previous quarterly report (GA-2747). The beginning-of-life shutdown margins are indicated in Table 2.1.

Corrections have been made for the steel spacers between control-rod compacts and for the 7-ft stroke which does not put the control rod completely into the 7.5-ft core. Transport-theory cell calculations indicate that an emergency rod, which has a poison compact of smaller diameter, is worth 17% less in $\Delta\rho$ than a control rod.

The reactivity worth of individual rods and of groups of rods depends significantly on the number and positions of other rods present. Table 2.2 shows the worth of the three rods in ring 3 used for setback as a function of the number of regulating rod groups in the central rings. The individual worths of three rods at the end of life as they are added in the central ring are given in Table 2.3. These rods would be the regulating group for the last several hundred days of life. The radial peak-to-average power density is also given, to indicate the peaking caused by unsymmetric arrangements.

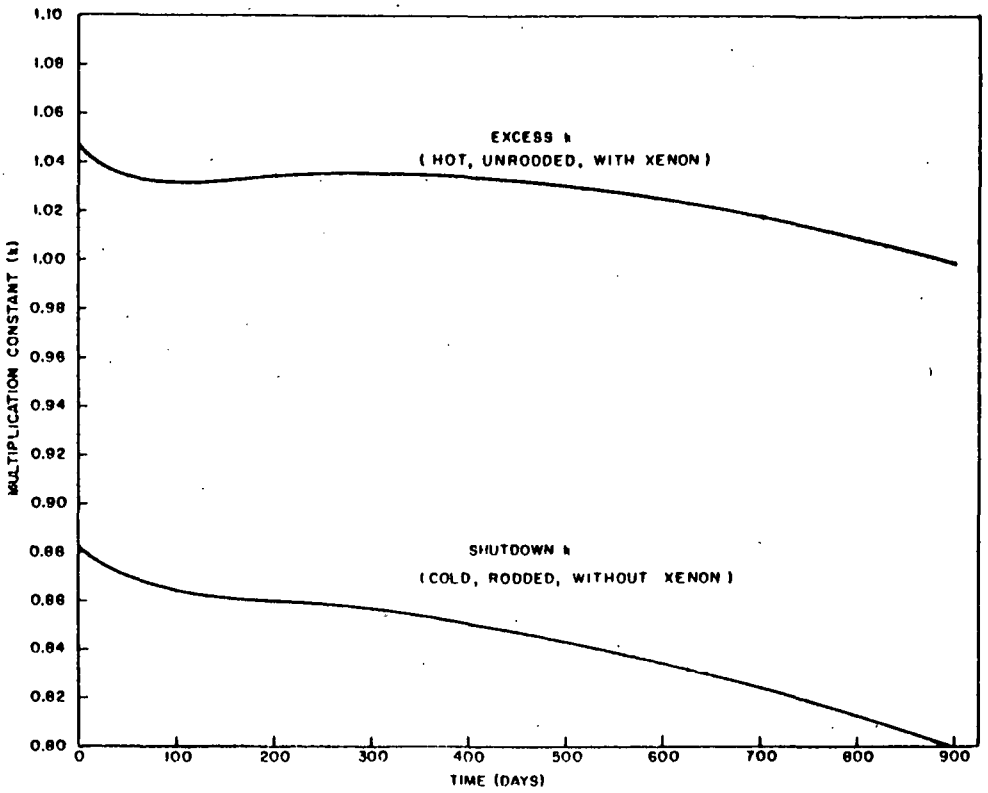

Fig. 2.3--Multiplication constant versus time of operation

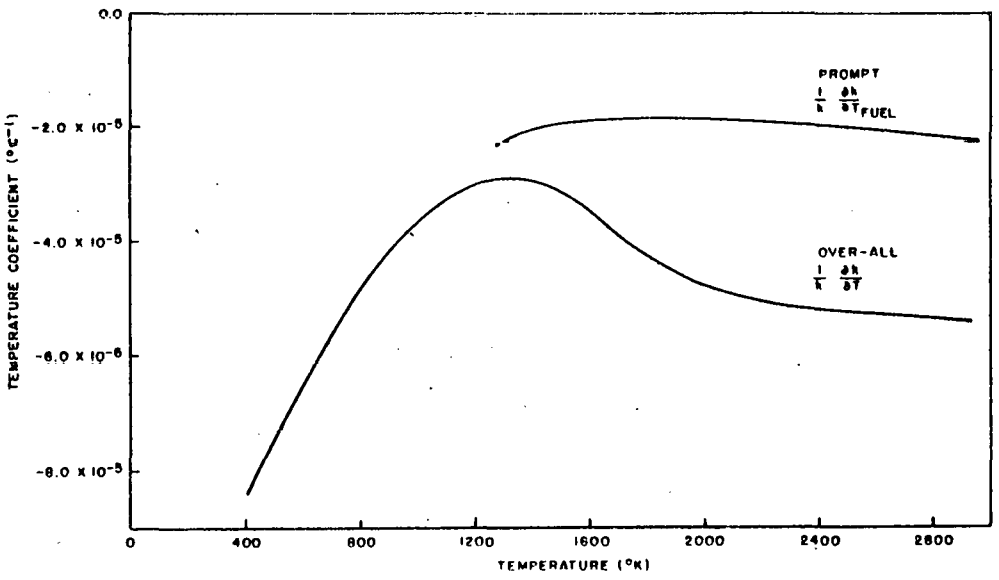

Fig. 2.4--Variation of temperature coefficient versus temperature at end of life with equilibrium xenon and samarium

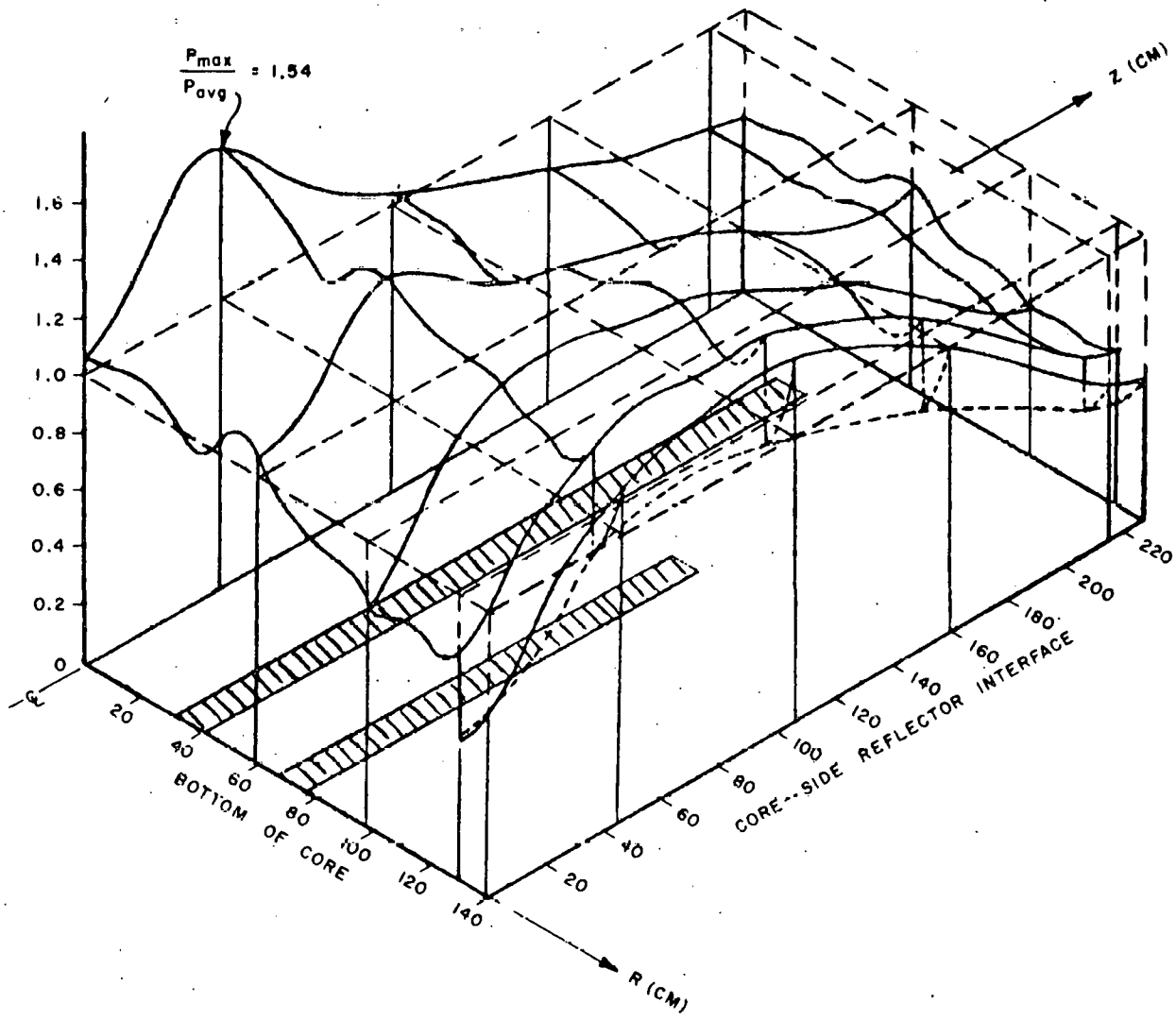

Fig. 2.5--Beginning-of-life power distributions (hot; critical; equilibrium xenon and samarium)

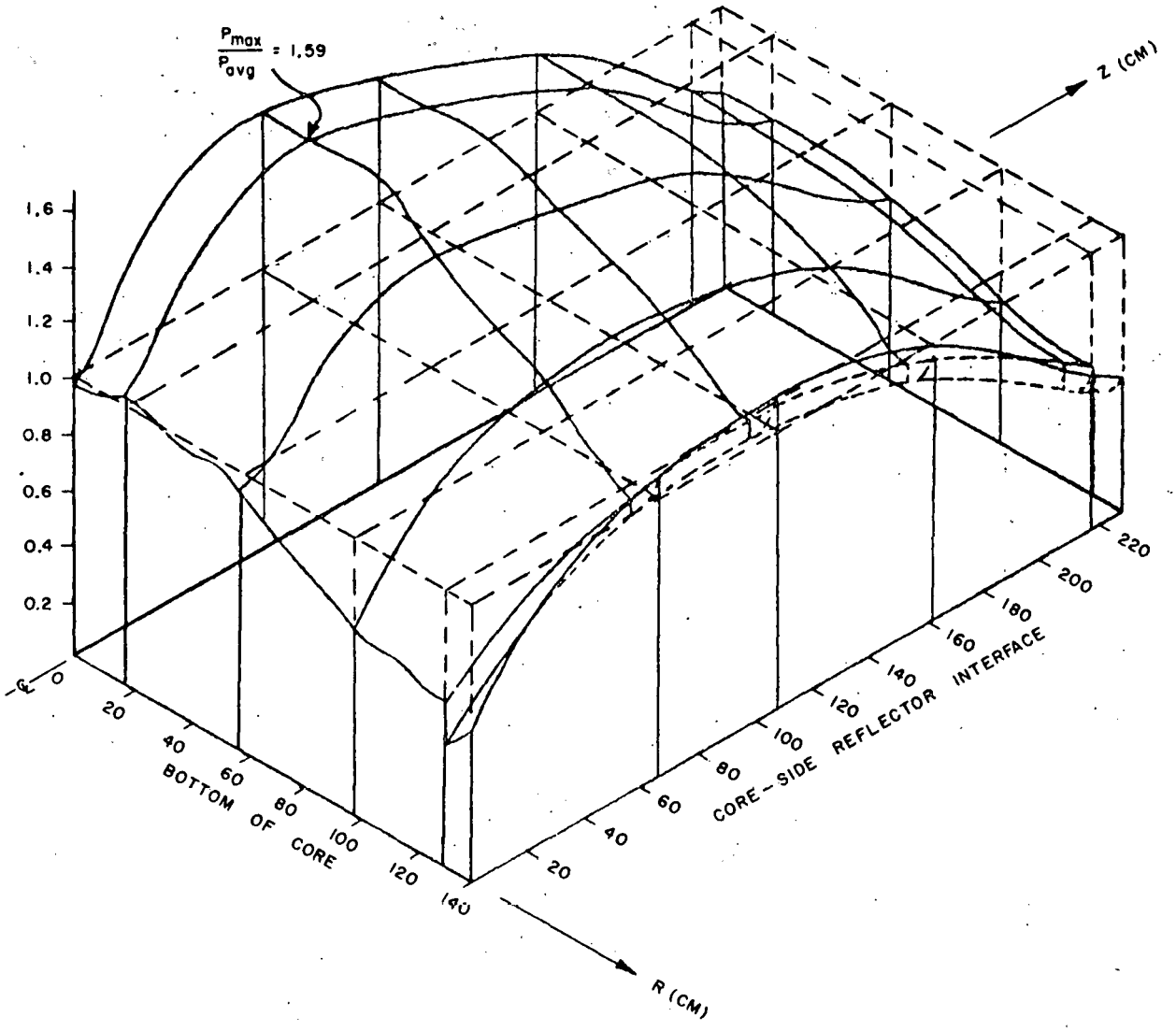

Fig. 2.6--End-of-life (900 days) power distributions (hot; critical; with no rods in core)

Table 2. 1

BEGINNING-OF-LIFE SHUTDOWN MARGINS

Number and Type of Rods Inserted	Effective Multiplication	
	300°K	1200°K
No rods	1. 148	1. 076
No rods, equilibrium Xe and Sm	1. 115	1. 046
36 control rods, no Xe or Sm	0. 890	0. 825
19 emergency rods, no Xe or Sm	1. 024	0. 956
55 thermal fuses, no Se or Sm	-----	0. 987

Table 2. 2

WORTH OF SETBACK RODS

Central Rods Present	Worth of Three Setback Rods ($\Delta\rho$)
None	0. 0147
Three in ring 1	0. 0182
Three each in rings 1 and 2	0. 0161

Table 2. 3

INDIVIDUAL WORTHS OF THREE RODS ADDED TO CENTRAL RING
(End of Life)

Number of Rods Added to Central Ring	$\Delta\rho$	$\hat{P}/\bar{P}$
0	-----	1. 32
1	0. 0097	1. 33
2	0. 0095	1. 37
3	0. 0099	1. 19

Reactor Kinetics Studies

The changes made in the initial core loading influence the dynamic behavior of the reactor in several ways. The reduction in thorium loading and the increase in rhodium loading result in a slight weakening of the negative temperature coefficient at operating conditions and in a considerable enhancement of the negative coefficient at high temperatures. A small reduction in neutron lifetime and an increase of the delayed-neutron fraction result from the increase in U^{235} inventory that persists throughout the life of the reactor.

Transients caused by the withdrawal of a particular control rod depend, of course, on the worth of this withdrawn rod. Detailed control-rod-worth calculations indicate that the largest worth of any single rod in the control-rod program will be 0.01 $\Delta\rho$ at the end of life.

A re-evaluation of the heat-transfer characteristics of the steam generator has resulted in an increase of the helium flow rate and a corresponding reduction in gas and fuel-element temperatures. The effect of these design changes on transients has been studied by recalculating the rod-fall incident. It is postulated that a rod of maximum worth (0.01 $\Delta\rho$) falls, under gravity, out of the core from its fully inserted position. The results are summarized in Table 2.4, together with corresponding values reported previously. The temperature versus time history for different scram conditions is shown in Fig. 2.7.

2.2. REACTOR ENGINEERING ANALYSIS

The system activities for the Peach Bottom reactor have been recalculated using the tentative release curve obtained from the in-pile-loop experiment. This new calculation gave results which are essentially in agreement with the beginning-of-life values listed in the Preliminary Hazards Summary Report.

A complete package of fuel element specifications and associated drawings was issued. This package is to provide the basis for procuring materials and for planning production operations.

A purge-flow-filter and rate-control plug was designed and tested. The new design utilizes grade 40 graphite filter material for a plug 4 in. long and 1-3/4 in. in diameter, for inclusion in the upper reflector of the fuel element. This arrangement replaces the design wherein the full upper reflector graphite acted as a filter. Laboratory tests on three units of the new design showed that the purge flow rate can be closely controlled at the required pressure drop through the plug. The plugs showed no change in flow rate after thermal cycling.

Table 2.4

SUMMARY OF ROD-FALL INCIDENT
(Rod worth 0.01 Δρ; 1.0 g acceleration)

Assumed Action	Maximum Fuel-compact Temperatures			Maximum Helium Outlet Temperatures	
	Average Element (°C)	Hottest Point (°C)	Time After Accident (sec)	°F	Time After Accident (sec)
Normal scram at 140% power	969 (1085)[a]	1380 (1504)[a]	0.63 (0.589)[a]	1326 (1384)[a]	1.0 (4.68)[a]
Helium-overtemperature scram at 1450°F	1487	2167	4.21	1575	23.4
Emergency scram after 30 sec	1487 (1554)[a]	2167 (2207)[a]	4.21 (2.9)[a]	1690 (1750)[a]	40.1 (41.0)[a]
No scram	1487 (1554)[a]	2167 (2207)[a]	4.21 (2.9)[a]	1743 (1781)[a]	~320 (96.6)[a]

[a]The values in parentheses indicate the numbers reported in GA-2493.

A specification and associated drawings have been prepared defining the fuel-element instrumentation requirements. Thirty-six instrumented fuel elements each contain two thermocouples. In addition, eight of these fuel elements contain acoustic thermometers. The axial and radial position of the fuel elements is varied, depending upon the purpose and location within the core.

2.3. EXPERIMENTAL ENGINEERING

A full-size fuel element was tested in an autoclave wherein full purge flow was maintained while the element was at reactor pressure and temperature. A mechanism which was to inject graphite dust into the purge stream apparently failed early in the 200-hr test. Therefore, the test is being rerun with a redesigned dust injector. The purge flow rate was kept at 1.1 lb/hr during the 200-hr run, and the pressure drop through the element stayed at approximately 4 psi.

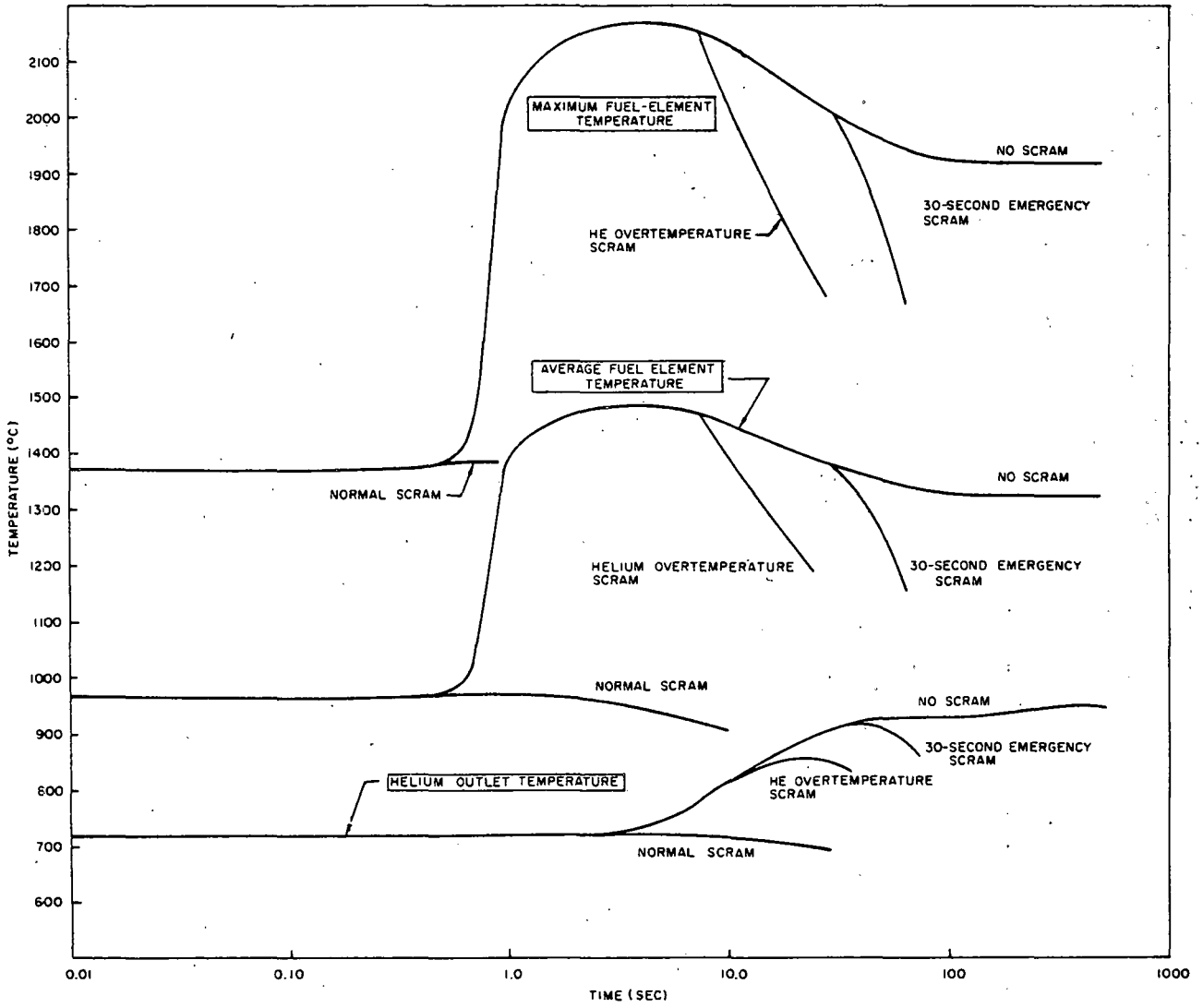

Fig. 2.7--Fuel-compact and helium outlet temperature following 0.01 $\Delta\rho$ rod drop (end of life; xenon present)

THIS PAGE

WAS INTENTIONALLY

LEFT BLANK

TASK IV. DEVELOPMENT OF REACTOR EQUIPMENT

4.1. CONTROL RODS AND DRIVES

During the quarter, the testing of the prototype control-rod drive was satisfactorily completed. The main purpose of the tests during this quarter was to confirm the design of the continuity-monitoring circuit and to demonstrate satisfactory operation of the fail-safe holding lock that will prevent a fully inserted control rod from inadvertently falling out of the core. The tests, in pure helium at reactor temperatures, showed that both these devices functioned properly.

At the conclusion of testing, the prototype drive had satisfactorily completed an over-all total of 590, 641 starts and stops, 5, 756 scrams, and more than 2. 6 million inches of random regulating motion in helium at reactor temperatures. These totals exceed the expected life requirements by a factor of 100 for the first two items and a factor of 1000 for the third.

After testing of the prototype control-rod drive was completed, modifications to the facility to permit the testing of the emergency shut-down rod and drive were started. Preparations were made for preliminary checkout of the system, which is scheduled for early next quarter.

4.2. FUEL-HANDLING EQUIPMENT

Flexing tests of an electrical cable in a high-temperature helium atmosphere were completed. The cable passed the rigorous test satisfactorily and has been selected for internal connections in the transfer machine.

THIS PAGE

WAS INTENTIONALLY

LEFT BLANK

TASK VI. DEVELOPMENT OF PLANT AUXILIARY SYSTEMS

6. 1. FISSION-PRODUCT CONTROL AND PRIMARY LOOP SYSTEM

Barium Permeation of Graphite Fuel- element Sleeves

Apparatus for the barium permeation experiment with a full-diameter, one-quarter-length fuel-element sleeve was completed, and preliminary calibration runs were started. Late in the quarter, this experiment reached operating temperature after a 3-day degassing period. The simulated fuel element was loaded with eleven full-size HTGR compacts stacked vertically inside an HLM-85 impregnated sleeve, as indicated in the sketch of the experimental apparatus (Fig. 6. 1). The sleeve has a helium permeability of 2×10^{-3} cm^2/sec. Four of the eleven compacts were made of graphite-matrix material only, while the other seven were impregnated with Ba^{133}-tagged BaO and untagged SrO to a 0. 6 mg/g carbon loading of both barium and strontium. Each tagged compact contained about 1 mc of Ba^{133}. The seven tagged compacts were placed in the center of the eleven-compact array.

In calibration experiments, a temperature survey was made of the compacts and sleeve while the sleeve was maintained at 1000°C. The temperature of the central heating element was found to be 1484°C. The survey was made by pulling a tungsten-rhenium sheathed thermocouple through a series of 1/16-in. -diameter holes drilled into each compact. The compacts used for the survey were, of course, not loaded with Ba^{133}. Temperatures were obtained for each compact at points on the inside, in the middle, and in the purge groove. A radiation pyrometer was used to obtain the outside sleeve temperature. Figure 6. 2 shows the profile obtained.

The element will be evaluated for barium distribution on the sleeve and the collectors at approximately one-month intervals until it can be shown that the system has reached an equilibrium distribution of barium. At that time, a series of corings will be made on all of the compacts and the sleeve to evaluate the over-all barium and strontium distribution.

The status of the barium diffusion, or better, permeation experiments with reduced-scale simulated fuel elements reported previously is given below:

1. Experiment No. 4 (impregnated HLM-85 base stock; helium permeability, $K_{He} \approx 2.4 \times 10^{-3}$ cm^2/sec at 1 atm) was terminated

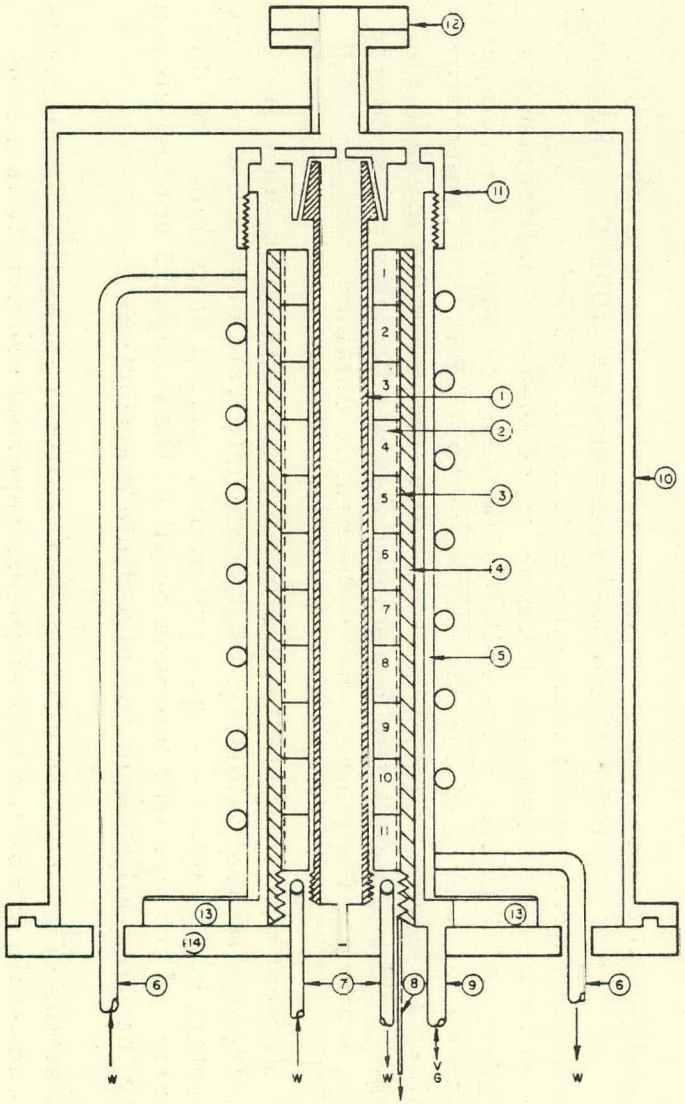

(1) AGOT graphite heating element (shaded)

(2) Full-size HTGR fue. compact; compacts 3 through 9 are loaded with 0. 6 mg Ba and Sr/g C (the barium is tagged with 1 mc Ba-133; both barium and strontium as the oxides

(3) Fuel-compact purge groove

(4) Full-diameter, 1/4-length graphite sleeve of 3/8-in. -thick, HLM-85 base stock (permeability, K = 2 × 10^{-3} cm^2/sec)

(5) Copper-cylinder water-cooled sink and electrode

(6) Water inlet and outlet for heat sink and electrode connection

(7) Water inlet and outlet for heat removal from end of sleeve and compacts; also acts as other electrode

(8) Exit purge-gas line from compact purge grooves

(9) Vacuum port; also serves as helium-gas inlet for filling containment vessel and purge

(10) Aluminum containment vessel

(11) Copper connector between heater element and electrode

(12) View port

(13) High-temperature epoxy-resin block for insulation of heat sink

(14) Brass base plate

Fig. 6. 1--Apparatus for barium permeation experiment with full-diameter, one-quarter-length sleeve

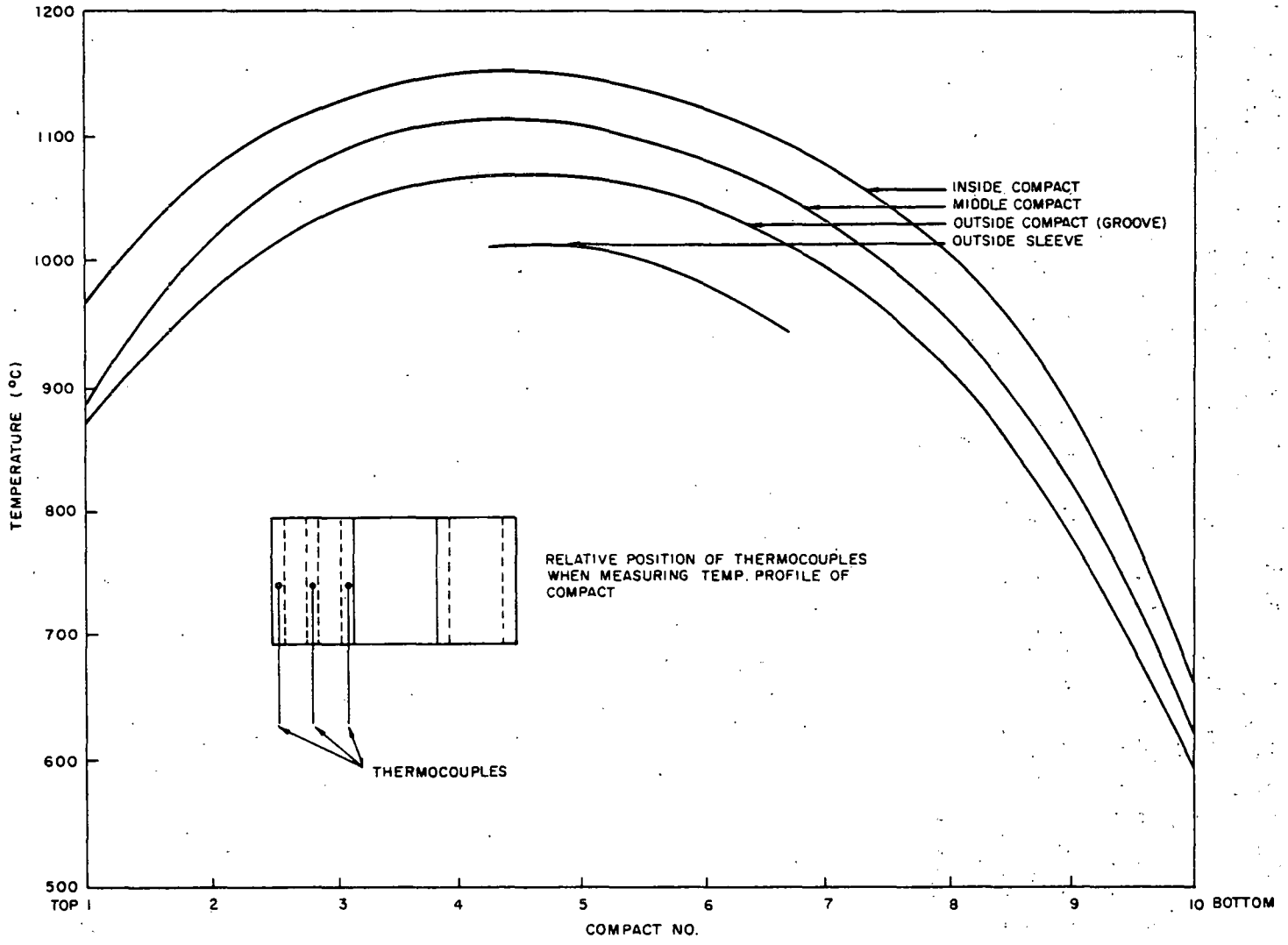

Fig. 6.2--Temperature profile of compacts and sleeve in barium permeation study of full-diameter sleeve

at 854 hr. Data on barium deposition quantities and rates were completely reported in the previous quarterly report (GA-3132).

2. Experiment No. 6 (HLM-85 base stock; $K_{He} \approx 2$ cm^2/sec at 1 atm) was terminated at 790 hr after four additional sampling periods. A coring of the sleeve will be made so that a radial barium concentration profile for the sleeve corresponding to terminal conditions will be obtained. The data obtained since the last report are given in Table 6.1.

3. Experiment No. 8 (impregnated HLM-85 base stock; $K_{He} \approx 2.4 \times 10^{-3}$ cm^2/sec at 1 atm) was terminated after 1491 hr. A coring of the sleeve will be made so that a radial barium concentration profile of the sleeve corresponding to terminal conditions will be obtained. Data obtained since the last report are given in Table 6.2.

Table 6.1

BARIUM PERMEATION EXPERIMENT--RUN NO. 6
Sleeve: Base stock HLM-85
Compact: Previously used in Run No. 4
Experimental Temperature: 1000°C
Carrier Helium Flow: 300 cm^3/min
Helium Permeability: ~2 cm^2/sec

Run No.	Δ Time (hr)	Accum. Time (hr)	Amount of Barium Deposited					
			Sleeve		Cold Finger		Stainless Sheet	
			Total Accum. (μg)	Rate (μg/hr)	Total During Sample Period (μg)	Rate (mμg/hr)	Total During Sample Period (μg)	Rate (mμg/hr)
6-11	87.75	577	1108	----	4.10	46.7	0.0064	0.073
6-12	69.5	664.5	1264	2.34	4.14	59.6	0.0015	0.022
6-13[a]	56	702.5	----	----	6.47	115.5	0.0006	0.011
6-14	87.75	790.25	----	----	8.08	92.1	0.0015	0.017

[a]Compact removed.

Barium permeation experiment No. 9 has run thus far for a total of 487.5 hr, using a compact loaded with 0.6 mg of strontium per gram of carbon and 0.6 mg of barium per gram of carbon tagged, respectively, with Sr^{85} and Ba^{133}. Barium and strontium were added to the compact as the oxides rather than the carbonates because of the higher reaction rate of the former with carbon. The sleeve material is HLM-85 impregnated base stock, and the experimental conditions being used are a temperature of

Table 6.2

BARIUM PERMEATION EXPERIMENT--RUN NO. 8

HLM-85 base stock, impregnated
2.4×10^{-3} permeability H-3
General Atomic heat-treated to final temperature 2800°C
Compact material: AGOT graphite
Compact length: 3 in. (2-1/2 in. loading)
New compact: (no previous heating)

Compact loading: Ba^{133}-tagged barium carbonate mixed with carbon (0.6 mg Ba/g carbon)
Experimental temperature: 1000°C
Carrier helium flow: 300 cm^3/min

Run No.	Δ Time (hr)	Accum. Time (hr)	Amount of Barium Deposited						Remarks
			Sleeve		Cold Finger		Stainless Sheet		
			Total Accum. (μg)	Rate (μg/hr)	Total During Sample Period (μg)	Rate (mμg/hr)	Total During Sample Period (μg)	Rate (mμg/hr)	
8-5	39	170.5	463.2	5.73	1.23	31.5	0.067	1.7	Changed back to impreg. sleeve, H-3 (samples 8-3 and 8-4 were run with nonimpreg. HLM-85)
8-6	44	214.5	750.7	6.53	41.5	943	0.172	3.9	
8-7	64.5	279	1252.6	7.78	14.6	226.4	0.39	6.0	
8-8	146.25	425			31.5	215.4	0.203	1.4	Compact removed
8-9	93	518			6.2	66.7	0.093	1.0	First sleeve coring for Ba distribution
8-10	36	554			5.5	154.0	0.082	2.3	Furnace was shut off automatically; 36-hr run assumed
8-11	135	689			20.3	150	0.174	1.29	
8-12	67	756			3.29	75.6	0.040	0.92	
8-13	135.75	892			6.49	47.9	0.119	0.88	
8-14	191.3	1083			12.49	65.3	0.0485	0.25	
8-15	52.4	1136			10.6	202.2	0.014	0.27	
8-16	139.3	1275			9.72	69.8	0.018	0.13	
8-17	215.8	1491			1.00	4.63	0.060	0.28	Terminated; second sleeve coring taken

1000°C and a helium carrier-gas flow of 300 cm^3/min. To date, eight experimental runs have been completed, but problems in analysis have arisen because both the barium and strontium are tagged. Analysis of the runs is being made on 256-channel analyzers and single-channel pulse-height analyzers, but, because the Sr^{85} back-scattering peak falls in the Ba^{133} photopeak energy range, the amounts of barium that have been deposited on the sleeve, stainless steel collecting sheet, and cold finger have not yet been determined. New methods of analysis are being worked on and should be completed shortly. After 255.3 hr of running time, a total of 684.2 μg of strontium has been evaporated to the sleeve material, with barium present in a small but unknown amount. The amounts of barium and strontium deposited on the cold finger and on the stainless steel collecting sheet (foil) are now being evaluated. Preliminary data show these amounts to be very low. Thus, very recent data on run No. 9-8 indicate deposition rates of 1.17 mμg Sr/hr and <0.1 mμg Sr/hr on the cold finger and stainless steel foil, respectively. The amount of Ba^{133} activity collected was so low that it was not measurable; thus, negligible quantities of Ba were deposited.

Concentration Profiles. The sleeves used in barium permeation experiments No. 4 and No. 8 were cored at termination and at 518 hr, respectively, to determine the distribution of barium through the sleeve wall. Four 1/8-in.-diameter holes were drilled 90 degrees to each other in the central part of the 1-in.-O.D. graphite sleeves. The holes were drilled stepwise through the 1/8-in.-thick sleeve so that five sample increments were obtained. These samples were then evaluated for barium content by comparison to a standard on a single-channel gamma spectrometer. The concentrations obtained are expressed in milligrams of barium per gram of carbon and are plotted in Figs. 6.3 and 6.4 versus distance from the outside surface of the sleeve. It is to be noted that the concentration profiles have a very pronounced S-shape on the semilog plot, with the concentration of barium on the outside of the sleeve about two orders of magnitude lower than that on the inside. The shape is far different from the linear slope expectation for steady-state permeation (assuming a constant diffusion coefficient) and is suggestive of the S-shaped breakthrough curve observed in dynamic-flow experiments where gas molecules are being eluted through an absorbent bed by an inert carrier gas. It is questionable whether a steady state has been reached in experiments No. 4 and No. 8. Experiments of longer duration where the barium-generating compact is retained in the sleeve and where successive corings are taken to give concentration profiles as a function of time should throw light on this question. The profile obtained from the corings of experiment No. 8 taken after 1491 hr, when compared with Fig. 6.4, should indicate whether or not appreciable diffusion occurs after the compact is removed.

It is to be noted the barium concentration profiles taken at the end of experiment No. 3 (unimpregnated HLM-85 graphite sleeve) as given in

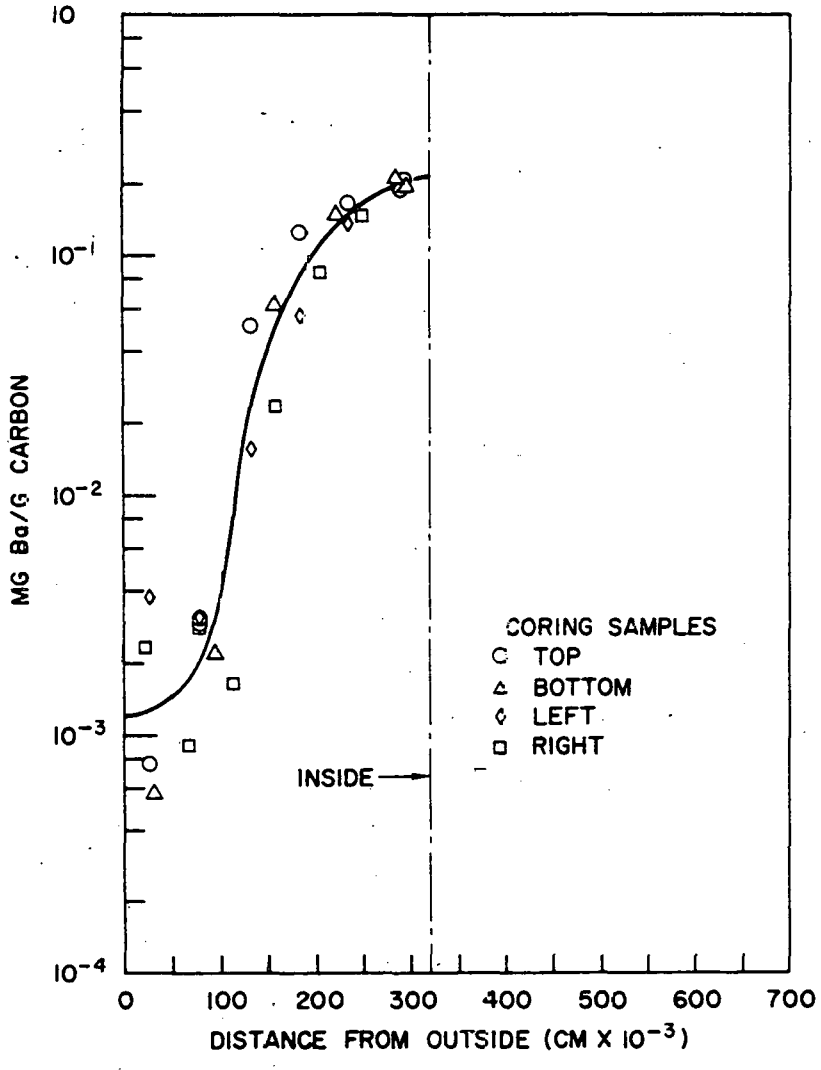

Fig. 6.3--Radial barium concentration profile (impregnated HLM-85 graphite; experiment No. 4)

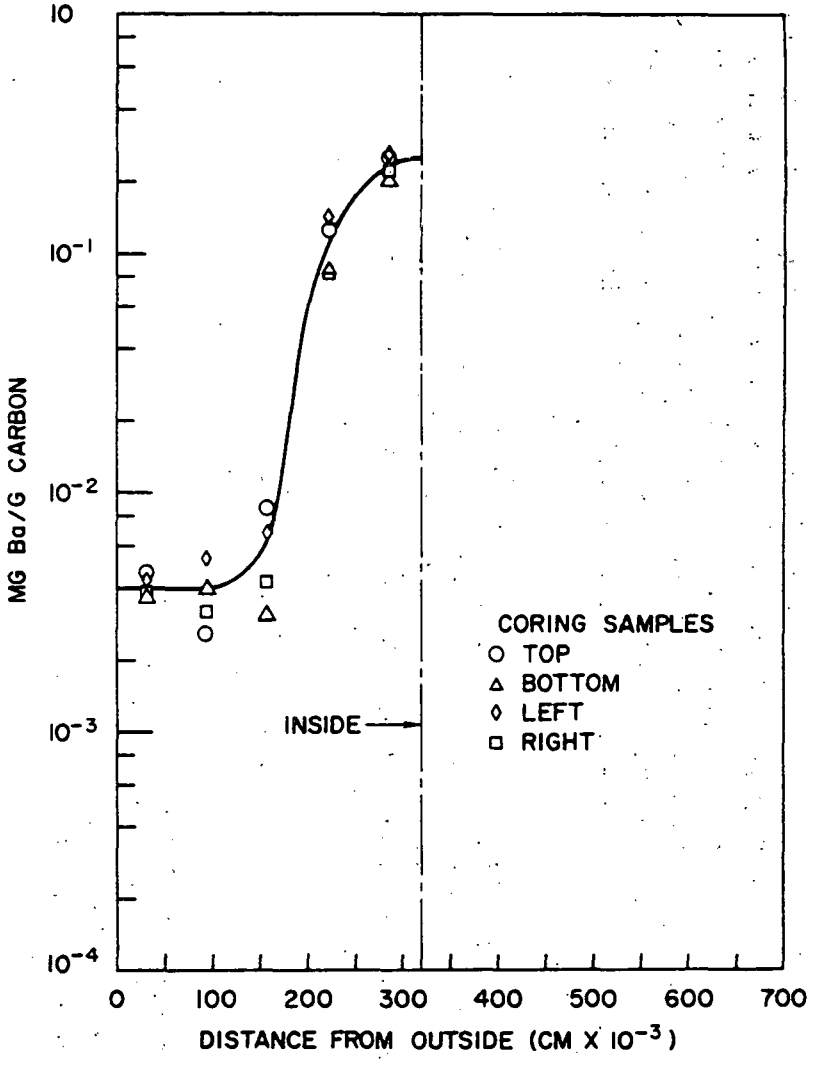

Fig. 6.4--Radial barium concentration profile (impregnated HLM-85 graphite; experiment No. 8)

Fig. 6.6 of GA-3132, the previous quarterly report, although not linear did not have a pronounced S-shape. In this case, the inside concentration was only about a factor of three higher than the outside. Also, the evaporation rate (to the tantalum or stainless steel collector foil) was quite large--order of 100 mμg at 900°C--and indeed was of the same order as the evaporation rate from the inside of the sleeve (see Table 6.5 of GA-2861 and pp. 84-86 of the same report).

Estimated Barium Partial Pressures and Apparent Permeation Coefficients. Employing the method described in quarterly report GA-2861 (pp. 85 and 86), the partial pressure of barium at the inside and outside of the sleeves in experiments Nos. 4 and 8 are estimated from observed evaporation rates. The barium evaporation rate, m/t, is given by

$$\frac{m}{t} = \frac{2\pi\ell}{\ln(a/b)} D_{12} \frac{\Delta P}{RT} ,$$

where ℓ = length of barium-loaded section of sleeve (6.3 cm);
a = outside diameter of region;
b = inside diameter of region;
a/b = 0.75 in./0.50 in. = 1.5, for inside;
a/b = 1.5 in./1 = 1.5, for outside;
$\Delta P \approx P_{Ba}$ = pressure at sleeve wall; and
D_{12} = barium–helium mutual diffusion coefficient, which is estimated (see p. 84, GA-2861) to be

$$D_{12} = \frac{0.41}{p} \left(\frac{T}{273} \right)^{1.75} \quad cm^2/sec .$$

The data used are the approximate, average rates of evaporation to the outer collector foil and to the cold finger (which, after the removal of the barium-containing compact, is extended so that it is axially located relative to and contiguous with the entire length of the central section of the barium-loaded sleeve). For the time period near the end of the experiments, the average evaporation rates to the cold finger (~30°C) were, for experiment No. 4, 140 mμg/hr and, for experiment No. 8, 130 mμg/hr. For these two experiments, the evaporation rates to the collector foil (~200°C) were 0.15 and 1.4 mμg/hr, respectively.

The estimated partial pressures, P_{Ba}, and corresponding concentrations, Q_{Ba}, based on the concentration-profile determinations mentioned above are listed in Table 6.3.

When more P_{Ba} and Q_{Ba} data of this sort are available from additional experiments (including experiment No. 6), the relationship between P_{Ba}, Q_{Ba}, and T as given in Eq. (6.1) of GA-3132 will be re-evaluated, assuming it applies. It agrees only very roughly with the above data.

Table 6.3

ESTIMATED BARIUM PARTIAL PRESSURES AND CORRESPONDING CONCENTRATIONS FROM EXPERIMENTS NOS. 4 AND 8

Experiment No.	Temp. (°C)	Inside Surface of Sleeve		Outside Surface of Sleeve	
		P_{Ba} (atm)	Q_{Ba} (mg Ba/g C)	P_{Ba} (atm)	Q_{Ba} (mg Ba/g C)
4	1000	1.5×10^{-10}	2.1×10^{-1}	0.92×10^{-15}	1.2×10^{-3}
8	1000	1.4×10^{-10}	2.5×10^{-1}	0.86×10^{-14}	4.0×10^{-3}

It is of interest to see what is the order of magnitude of the permeation coefficient, K, for flow through the graphite sleeve defined by

$$\frac{m}{t} = K \frac{2\pi\ell}{\ln(a/b)} \frac{\Delta P}{RT} ,$$

where m/t = the rate of flow of barium through the sleeve which equals the rate of deposition on the outer collector foil,
ℓ = length of barium-loaded section of the sleeve,
a/b = O. D. of sleeve divided by I. D. of sleeve = 1 in./0.75 in. = 1.33,
ΔP = pressure drop of barium across sleeve, and
T = temperature of sleeve.

The permeation coefficients, K, calculated on the basis of the above data and a temperature of 1273°K, are 1.6×10^{-3} cm^2/sec for experiment No. 4 and 1.6×10^{-2} for experiment No. 8. The value of K for experiment No. 4 is seen to be of the order of magnitude of the permeability coefficient one might estimate from the helium permeability, $K_{He} \cong 2.4 \times 10^{-3}$; thus, assuming that a $(T/M)^{1/2}$ correction approximately applies, we estimate

$$K \approx K_{He} \left(\frac{1273}{273} \times \frac{4}{137} \right)^{1/2} \approx 0.9 \times 10^{-3} .$$

In the case of experiment No. 8, a loss rate from the sleeve which is an order of magnitude higher is obtained. This higher loss rate, if real, must be due to some other mechanism than gas-phase in-pore diffusion, i. e., in-pore surface diffusion or a bulk diffusion process. It is hoped that further experiments will throw light on the nature of the transport processes involved.

Vaporization of Barium from Graphite

Knudsen Cell Experiments. The study of the vapor pressure of barium

in equilibrium with polycrystalline graphite has continued. The Knudsen cell technique has been applied to specimens of HLM-85 base-stock graphite containing approximately 0.2 mg Ba/g graphite; the Ba was tagged with Ba^{133}. The graphite specimens were taken from a King furnace heating element (reduced-scale, simulated, fuel-element sleeve) which had been used in a barium permeation experiment (No. 3). The specimens were ground to fine powders for the Knudsen cell measurements. The technique used was to heat a specimen at 1000°C and to collect a portion of the effusate from a molybdenum Knudsen cell on a graphite target. The target was then removed and counted, during the counting time the barium-containing graphite being exposed to the atmosphere. Three other specimens were similarly tested at temperatures of 1100°, 1200°, and 1300°C. The observed vapor pressures showed the following characteristics: There was no clear dependence on temperature, the scatter was large, and the pressure decreased fairly continuously from one run to the next. The decrease in pressure is probably not due to the depletion of barium within the Knudsen cell; the barium content decreased by 30% at most, while the observed vapor pressures fell off by an order of magnitude or more. It is difficult to interpret these results. It may be that there is still an uncontrolled variable in the experiments. Several more runs were made in which the exposure of the cell to the atmosphere was kept to a minimum by backfilling the system with argon. However, a simple calculation shows that it is virtually impossible to break the vacuum in the Knudsen cell furnace without admitting a significant amount of oxygen compared with the small amount of barium present.

A further test was made to study the possibility that diffusion of barium in the graphite particles within the Knudsen cell was the rate-controlling process. If diffusion in these particles were very slow, the saturation pressure of barium in the cell would not be attained and one would expect a nonuniform distribution of barium within the particles. Such a nonuniformity would manifest itself as a particle-size-dependent concentration of barium in the graphite particles. Accordingly, a sample of barium-impregnated graphite was ground to a powder and screened into several size ranges from 37 to 177 μ. In this experiment, the barium concentration showed no dependence on particle diameter, indicating that the barium was rather uniformly distributed within the particles.

Transpiration Experiments. Three runs attempting to determine the vapor pressure of barium over barium-containing HLM-85 graphite base stock at 1000°C were made during the quarter. In these transpiration experiments, inconclusive results were obtained for barium loadings of 0.37, 0.74, and 1.45 mg Ba/g C with a helium flow rate of about 100 cm^3/min, since after about 400 hr no further transport of the barium could be detected. Preliminary estimated barium pressures of 7×10^{-11} and 2×10^{-10} atm were observed for loadings of 0.37 and 0.74 mg Ba/g C. No reasonable

estimate of the barium pressure could be obtained for a loading of 1.45 mg Ba/g C.

Diffusion and Sorption of Barium in Graphite

Barium Diffusion in Pyrographite. Experiments have been undertaken to study the diffusion of barium in pyrolytic graphite. The graphites used have been plates of 1/8-in.-thick material. Disks (3/4-in.-diameter) were cut from these plates, and suitable caps were prepared from the same material. Barium containing Ba^{133} was deposited on the surface of the disk by evaporating from a $Ba(NO_3)_2$ solution. The disks were heated to 1000°C in a vacuum furnace with the caps in place to reduce the evaporation rate of barium. Since the order of magnitude of the diffusion coefficient of barium in pyrographite is not known, three exploratory experiments were carried out with the HTM material for times of 2, 46, and 217 hr. The samples were sectioned and analyzed radiochemically for barium. The barium penetration perpendicular to the planes of the pyrographite was so small as to be indeterminate, even in the longest run, indicating a diffusion coefficient of much less than 10^{-6} cm^2/sec in this direction. The entire surface of the disk was found to contain barium, however, indicating an extensive surface migration.

Two subsequent diffusion anneals were carried out at 1000°C for 226 hr, one with GE and one with HTM pyrographite. After the anneal these specimens also had barium over the entire surface. No barium was deposited on the curved surface of these disks and the barium found there arrived by an apparently rapid surface-diffusion phenomenon. The specimens were sectioned both parallel and perpendicular to the orientation of the layer planes. Results showed that the diffusion parallel to the planes is much faster than that perpendicular to the planes. Analysis of the data obtained to date yielded the following diffusion coefficients for barium in graphite at 1000°C: GE pyrographite, 1×10^{-10} and $\sim 1 \times 10^{-11}$ cm^2/sec for directions parallel and perpendicular, respectively, to the planes; HTM pyrographite, $\sim 1 \times 10^{-11}$ and $< 5 \times 10^{-12}$ cm^2/sec for directions parallel and perpendicular to the planes. These values are approximate, except the value for the GE specimen in the parallel direction, for which a good concentration profile was obtained.

Thus it appears that at 1000°C diffusion coefficients of the order of 10^{-10} to 10^{-11} cm^2/sec apply to the bulk diffusion of barium atoms in the direction parallel to the carbon hexagonal-network layer structure of the pyrolytic graphite.

Sorption of Barium in Graphite. A 1000-hr static barium sorption run (1000° to 700°C) on an 8-in.-long cylinder of HLM-85 base-stock graphite was completed during the quarter. The apparatus used is as

described in GA-3132. The results of this run indicated that the barium supply had been exhausted and a portion of the sorbed barium on the graphite was distilled out of the top of the reaction tube. Thus the final barium vapor pressure is unknown. A concentration profile of the specimen showed a relatively uniform saturation of 1.0 mg Ba/g C at 1000°C, 2.2 mg/g at 800°C, and 1.9 mg/g at 720°C.

A similar run with a barium pressure of 10^{-6} atm scheduled for 720 hr is nearing completion.

Fission-product Release

In-pile-loop Element III-A Krypton and Xenon Release Data. Fission-product release data for element III-A were calculated and are shown in Fig. 6.5 as a plot of steady-state fractional release versus half life. The specific activities for Kr^{85m}, Kr^{87}, Kr^{88}, Kr^{89}, Xe^{133}, Xe^{135}, and Xe^{138} were measured using conventional multichannel gamma-ray spectrometry. The Kr^{89} and Xe^{138} were measured by observing the daughter products Rb^{89} and Cs^{138}.

During the 133 Mw-hr of element III-A loop operation, the release fraction increased by roughly one order of magnitude. This was due partly to a steady degradation of fuel and to the large fluctuations caused by many variables affecting release, such as fuel temperature, purge flow, and hot-spot position.

Measurements of the gross noble-gas fission products from both the purge stream and the main coolant loop showed roughly a factor of 1000 times less activity ($\mu c/cm^3$) in the main loop than in the purge stream.

Due to sampling problems associated with reactor and loop operations and analysis problems due to low count-rate samples and high background conditions, only a few analyses were adequate for the calculation of effective sleeve permeability. The data used for the calculation of the effective permeability for Kr^{85m} are:

Main-loop Kr^{85m} specific activity	2×10^{-3} $\mu c/cm^3$ at loop temperature and pressure
Purge-stream Kr^{85m} specific activity	2.62 $\mu c/cm^3$ at loop temperature and pressure
Indicated purge flow rate	0.47 lb/hr
Estimated loop volume	5×10^5 cm^3
Estimated helium gas inventory	1.64 lb
Mean area of fuel-element sleeve	2.5×10^3 cm^2
Thickness of fuel-element sleeve	0.95 cm

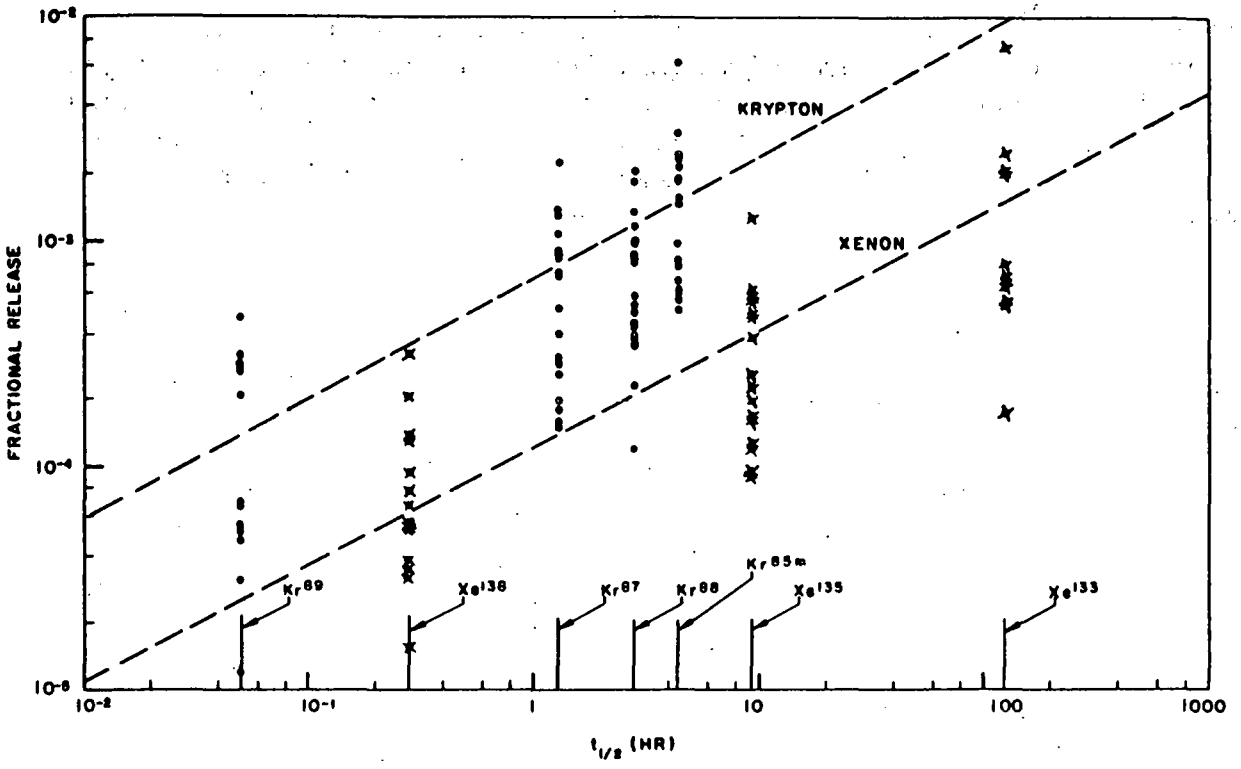

Fig. 6.5--Fractional release from element III-A versus half life

The ratio of the main-loop to purge-gas specific activity, A_L/A_P, at the steady state is directly related to the effective permeation coefficient, K_{eff}, of a given fission-product gas. Thus,

$$\frac{dN_i}{dt} = 0 = K_{eff}\left(\frac{A}{L}\right)\left(\frac{C_i}{2}\right) - \lambda_i N_i - RN_i ,$$

where N_i = atoms of noble-gas fission product i in loop;
K_{eff} = effective permeation coefficient of the noble gas, cm^2/sec;
λ_i = decay constant of i atoms, sec^{-1};
R = purification-system cycling rate (flow rate through purge system divided by inventory of helium), sec^{-1};
C_i = concentration of fission-product atoms i in purge (at exit of fuel element), $atoms/cm^3$;
A = mean area of the fuel-element sleeve, cm^2;
L = thickness of sleeve, cm; and
V_L = loop volume, cm^3.

Thus, the loop activity is

$$N_i\lambda_i = \frac{K_{eff}C_i\lambda_i}{2(\lambda_i + R)} \cdot \frac{A}{L} ,$$

and, since the specific activity ratio (of loop to purge activity) is

$$(A_L/A_P)_i = \frac{N_i/V_L}{C_i} ,$$

we have

$$K_{eff} = 2(A_L/A_P)_i (\lambda_i + R) (L/A)V_L .$$

Then, for Kr^{85m} we calculate the effective permeability of the III-A sleeve for krypton as 3.6×10^{-5} cm^2/sec. The sleeve temperature at the time the data were taken was roughly 1500°F.

In-pile-loop Element III-B Krypton and Xenon Release Data. Krypton and xenon fission-product release data for element III-B have been worked up covering three reactor cycles (approximately 100 Mw-hr of loop operation). The longer-lived isotopes had an over-all release-rate increase of about a factor of ten, while the shorter-lived isotopes increased by about a factor of one hundred.

No activity was detected in the main coolant gas by normal sampling procedures. However, in early May, larger gas samples were taken from the main coolant, at which time several of the isotopes of interest were detected. A calculation of the effective sleeve permeability was made with the data thus obtained. The following values for element III-A were used:

Main-loop Kr^{85m} specific activity	1.4×10^{-4} $\mu c/cm^3$ at loop temperature and pressure
Purge-stream Kr^{85m} specific activity	1.64 $\mu c/cm^3$ at loop temperature and pressure
Indicated purge flow rate	0.495 lb/hr

Other quantities were the same as for element III-A. The effective sleeve permeability for Kr^{85m} was calculated to be 4.1×10^{-6} cm^2/sec. The sleeve temperature at the time of the analysis was 1992°F. The K_{eff} value is of course only approximate, because of the uncertainties in the purge flow rate, loop volume, and helium inventory, as well as in determining the specific activity.

In May, 1962, a test was performed wherein the purge flow was stopped and the activities in the main coolant stream were allowed to reach an equilibrium point. The activity increase was observed both by extraction of individual gas samples with time and by the observation of a series of radiation monitors (ion chambers) situated throughout the loop. After the activity had reached what appeared to be a constant level, the purge flow was again started and set at an indicated flow rate of 0.54 lb/hr.

Both the radiation-detector readings and the gas counting showed the activities to have leveled off after about 12 hr with no purge flow. The largest buildup of activity was shown to have taken place in the first hour after stopping the purge flow. The de Havilland circulator was circulating the loop gas at the time of this test. The fuel temperature during the test was 2705°F on the hot side and 2415°F on the cold side; the sleeve cold-side temperature was 1992°F.

The gas samples taken during this test were first counted for gross noble-gas activity and then were counted on a multichannel gamma-ray spectrometer for the individual isotopic activities. Calculated on the basis of the highest specific activity result obtained during the test and a loop volume of 10 ft^3, the release fractions and gross isotope activities obtained in the loop are listed in Table 6.4.

Table 6.4

ACTIVITIES AND RELEASE FRACTIONS DURING NO-PURGE-FLOW TEST

Isotope	Specific Activity ($\mu c/cm^3$ at L. T. P.)	Gross Isotopic Loop Activity (curies)	Release Fraction from Main Loop; Max. During No-Purge-Flow Test	Release Fraction from Purge Gas; Prior to No-Purge-Flow Test
Kr^{85m}	2.5	0.708	7.5×10^{-4}	1.9×10^{-3}
Kr^{87}	1.99	0.563	3.3×10^{-4}	7.7×10^{-4}
Kr^{88}	1.66	0.47	1.9×10^{-4}	6.1×10^{-4}
Kr^{89}	$<10^{-4}$	-----	----	----
Xe^{135}	2.48	0.70	1.7×10^{-4}	6×10^{-4}
Xe^{138}	0.685	0.19	5.0×10^{-5}	----
		2.63[a]		

[a] Total gross isotopic loop activity.

The gross activity buildup resulting from the stopping of purge flow is shown in Fig. 6.6; the cleanup of the gross activity upon resumption of purge flow is shown in Fig. 6.7.

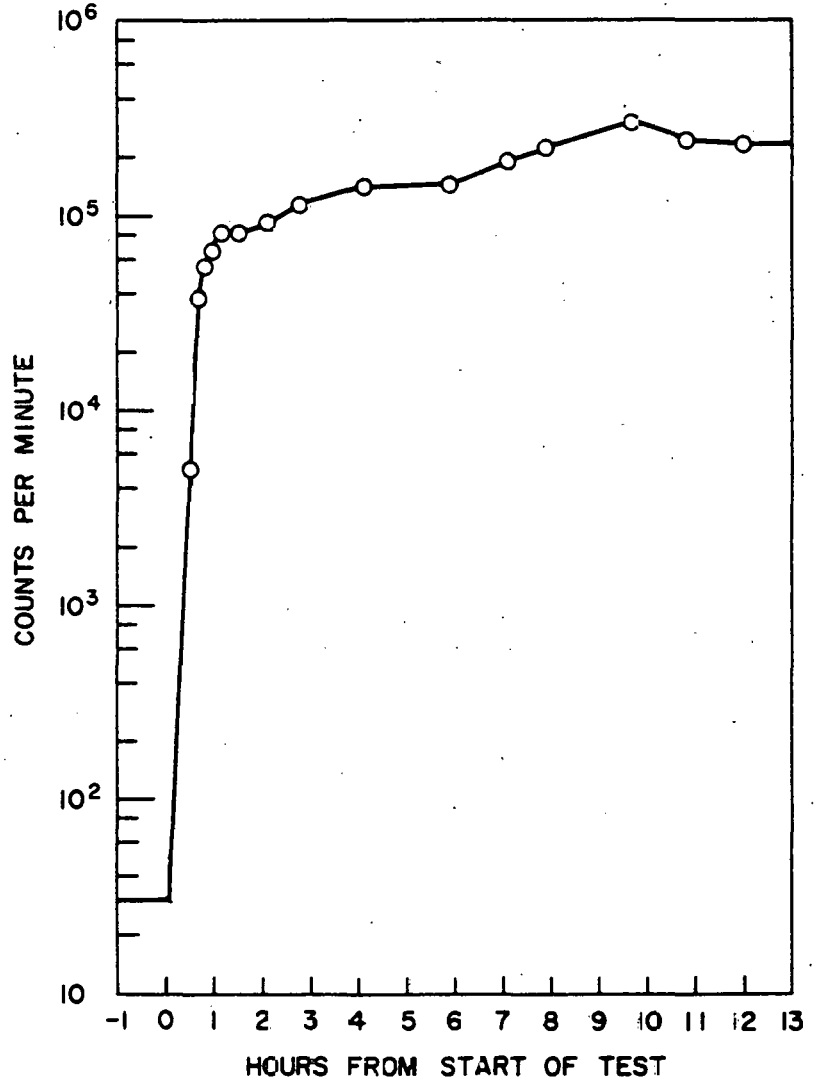

Fig. 6.6--Gross-activity (>200 kev) buildup during no-purge-flow test (element III-B)

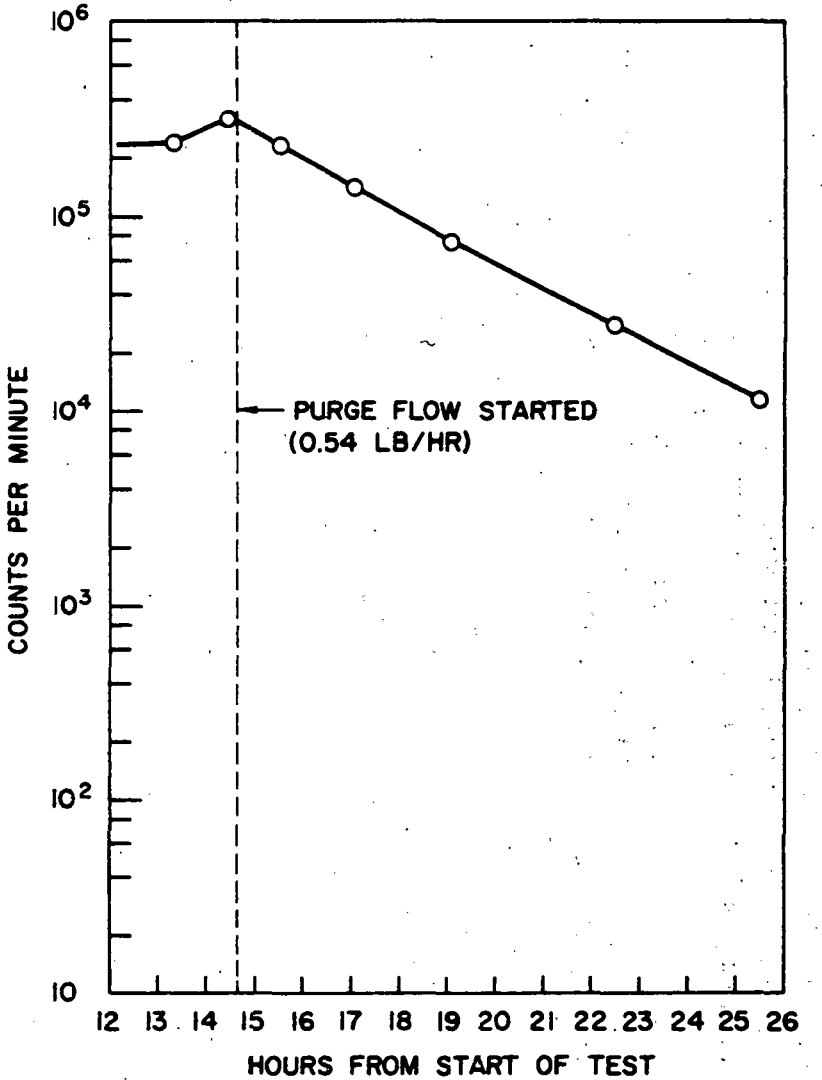

Fig. 6.7--Gross-activity (>200 kev) cleanup following no-purge-flow test (element III-B)

The total Kr and Xe activities measured equal 2.6 curies, whereas the gross activity result obtained by integral count above 200 kev (with estimated counting efficiency of 2%) is 6 curies.

Analysis of the cleanup half lives for the individual isotopes indicates that several basic loop parameters used may be in error. By using a loop helium inventory of 1.64 lb in place of 1 lb and a purge flow one-third of that indicated (or 0.18 lb/hr), one can calculate values for the cleanup ($t_{1/2}$ eff) that agree fairly well with the actual test results (Table 6.5). The 1.64-lb value was calculated from the cleanup of a nitrogen contamination of the main loop gas. The 0.18 lb/hr purge-flow value is arrived at by the comparison of release-fraction values from purge-stream data and main-loop (no-purge-flow) equilibrium data.

Table 6.5

COMPARISON OF EXPERIMENTAL AND CALCULATED CLEANUP RATES FOR NO-PURGE-FLOW TEST

Isotope	Experimental Cleanup Rate (hr)	Calculated Cleanup Rate[a] (hr)
Kr^{85m}	2.6	2.59
Kr^{87}	1.25[b]	1.04
Kr^{88}	1.5	1.94
Xe^{135}	4.1	3.73

[a]Assuming 1.64 lb helium and 0.18 lb/hr purge.
[b]Based on three data points only.

Distribution of Barium, Strontium, and Cesium in In-pile-loop Element III-A. A postirradiation analysis for fission-product distribution is under way, and some preliminary data have been assembled. The several components of the element assembly have been sampled in the General Atomic hot cell facilities and have been analyzed for content of Ba^{140}, Cs^{137}, Sr^{89}, Sr^{90}, and, in some cases, for I^{131}.

The internal trap has been sectioned and samples taken longitudinally along the outer surface. The results are still inconclusive at this time because of the difficulty in separating the isotopes from the large amounts of silver activity present (which results from the activation of silver in the trapping reagent to Ag^{110m}). There is an especially difficult problem in the separation of iodine activity from the silver activity.

Core samples 1/4-in. in diameter have been taken from the sleeve 6 in. apart longitudinally on both the hot side and the cold side. Each of these core samples was then sliced into five equal thicknesses to give radial sleeve samples at each longitudinal position sampled. There does not appear to be any particular profile pattern apparent at this time; there is some difficulty, however, in fitting a smooth curve to the data points.

Longitudinal and radial samples have also been taken from the central spine material for fission-product distribution, and samples have been taken from the fuel bodies for burnup analysis.

Distribution of Barium, Strontium, and Cesium in GA-309 Capsules. A postirradiation analysis for fission-product distribution is almost completed on the GA-309 series irradiation capsules. Capsules GA-309-4, -6, and -8 were selected for analysis in detail. The can and spine samples are 1/8-in.-wide lathe turnings taken at various depths. Cap samples are 5/8-in. core samples taken (coaxially with cap) to various depths.

In general, the isotope profiles appear to have at least one peak present. A leak in the containment after irradiation allowed water to enter the system, and it is not known what effect this had on the over-all profile. The final results of postirradiation examination are not complete at this time.

Annealing Experiments on Coated and Uncoated Particles of In-pile-loop Element III-C. Fission-product-release studies have been completed on two series (one PyC-coated and one uncoated) of element III-C particles. The fuel was prepared from the mixed oxide which had been converted to the carbide. Runs have been made at 1700°, 1400°, 1200°, and 1000°C for each series. Release data obtained for Xe^{133}, Ba^{140}, I^{131}, and Te^{132} are being processed.

Diffusion of Noble Gases Through Graphite

Room-temperature back-diffusion of argon, krypton, and xenon against a helium pressure differential was measured on a sample of GLI-S-15 sleeve-material graphite. The measurements of argon back-diffusion were made using pure helium and pure argon with mass spectrometric analysis. The krypton (Kr^{85}) measurements were made using a Dynacon vibrating reed electrometer–ionization-chamber instrument. In this case, very dilute krypton in helium back-diffused against pure helium. The difference in $K_{apparent}$ between krypton and xenon seems to increase with increasing ΔP, and the difference decreases with increasing $\overline{P}$ (see Fig. 6.8). It is interesting to note that the argon and krypton back-diffusion data at $\overline{P} \approx 3$ atm are essentially the same.

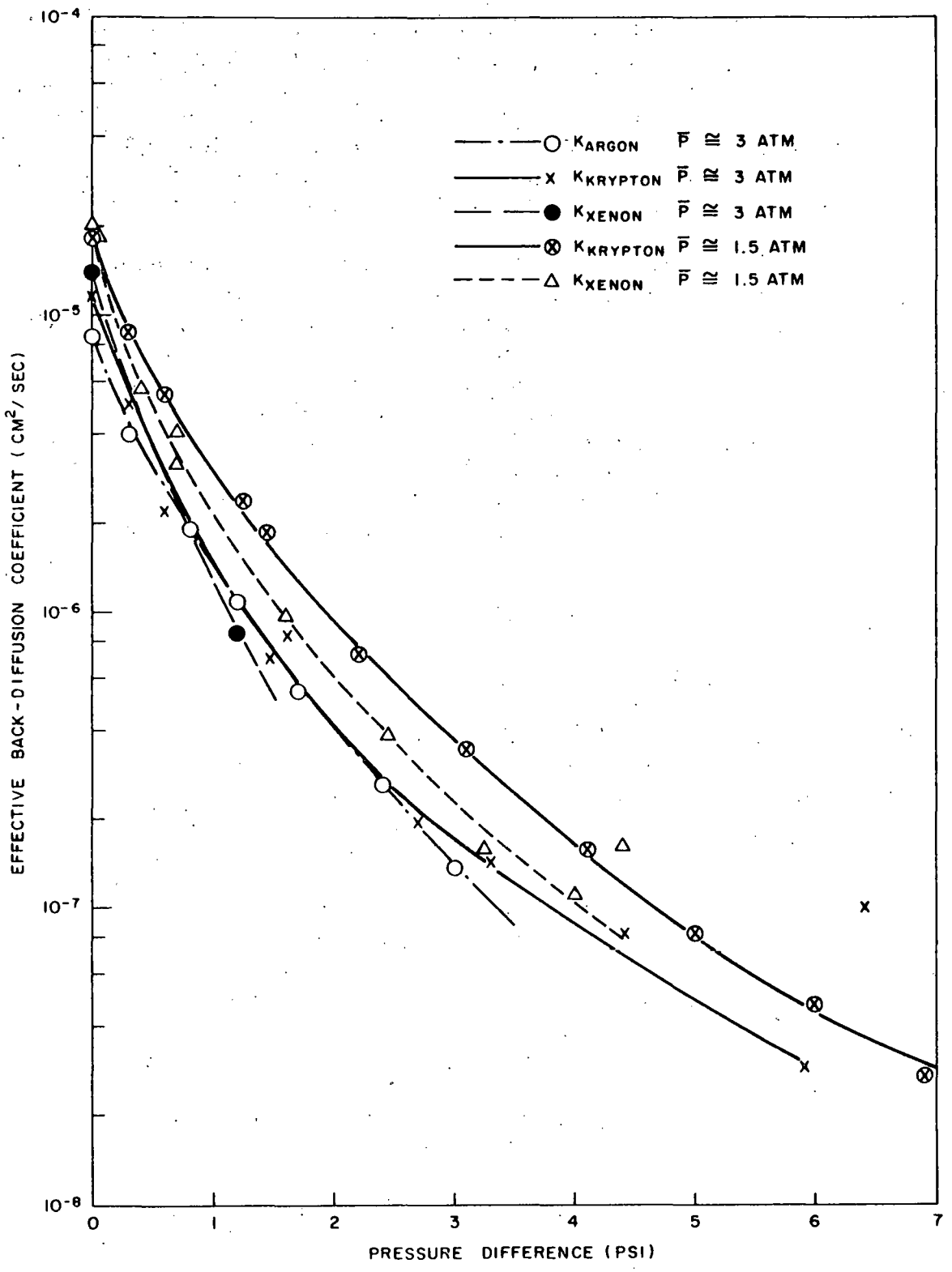

Fig. 6.8--Effective back-diffusion coefficient versus pressure difference (GLI-S-15 graphite)

A sample of National Carbon NCD3 sleeve graphite was tested. The helium permeability versus average pressure (see Fig. 6.9) shows a relatively high zero intercept. The krypton in helium back-diffusion versus differential pressure plot (see Fig. 6.10) shows a profile typical of National Carbon materials examined to date, i.e., a flat shape with a high order of back-diffusion. Both the high K_{He} intercept and the back-diffusion profile indicate a small-pore graphite and probably a narrow range of pore sizes.

Helium permeability versus average pressure measurements were made on a series of seven sleeve-material graphites. These were 3-in. lengths cut from sleeves which had been previously tested in the engineering-scale back-diffusion setup. These data were obtained to see if helium permeability data may be correlated with the back-diffusion results. Some of the results deviate considerably from the nominal permeabilities of the main tubes from which the specimens were cut. Differences of the order of a factor of ten have been noted before from separate samples taken from the main piece. These differences between samples removed from the end and from the middle may be due to the higher impregnating efficiency resulting from the anisotropic orientation along the tube main axis.

Fission-product Plateout and Decontamination Studies

Fission-product Plateout in the In-pile Loop. An attempt was made to identify Cs^{137} and Ba^{140} plateout in the in-pile loop. The survey made of the housing of the de Havilland circulator indicated ~100 μc of cesium per square foot of housing. No barium activity was found. Also, tantalum activity was low. A survey of the loop pipe between the filter and the strainer before the circulator indicated ~200 $\mu c/ft^2$ of Cs^{137} with no detectable Ba^{140}. Assuming 25 sq Å/atom comprises a monolayer (on the basis of the superficial or geometric external surface), an activity level of 100 $\mu c/ft^2$ corresponds to 0.014 monolayer of Cs^{137}. This is a negligible contamination level for the Peach Bottom reactor. An unsuccessful attempt was made to look for activity in the cooler. The cooler precedes the above-mentioned monitored areas. There is a high background in this area, due in part to Ta^{182} activity, which makes detection of Cs^{137} impossible. Other methods for the determination of barium and cesium plateout in the main loop are under consideration. This includes sampling by incorporation of bypass lines with water-cooled charcoal traps around the cooler and the other points in the primary coolant circuit.

Decontamination Studies. The decontamination and waste-processing systems for the Peach Bottom plant were reviewed. The optimum system appears to be one designed to handle a multistep decontamination process including the use of steam, basic and acidic reagents, and rinses. The exact process will be specified following additional decontamination tests.

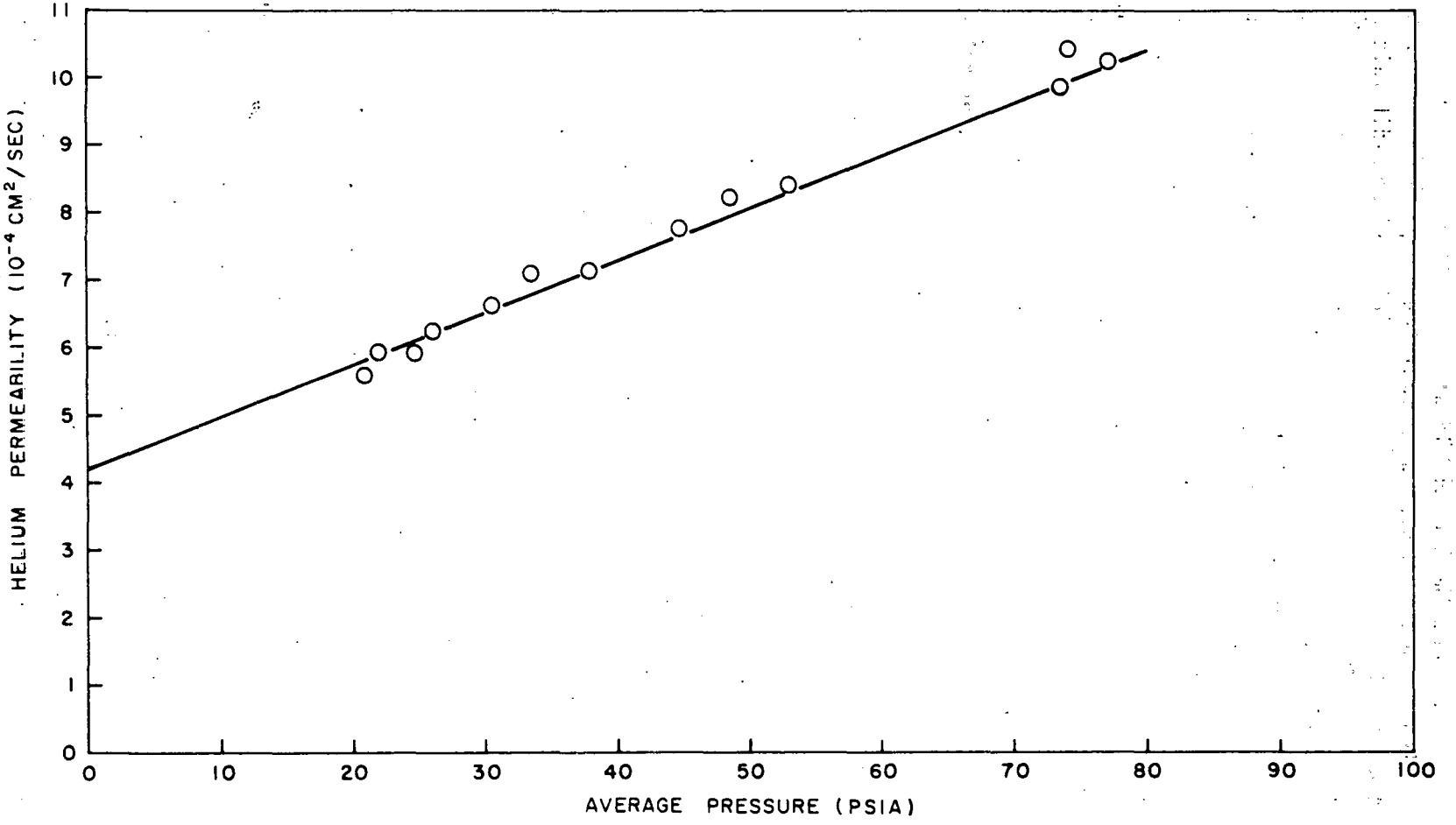

Fig. 6.9--Helium permeability versus average pressure (NCD3 graphite)

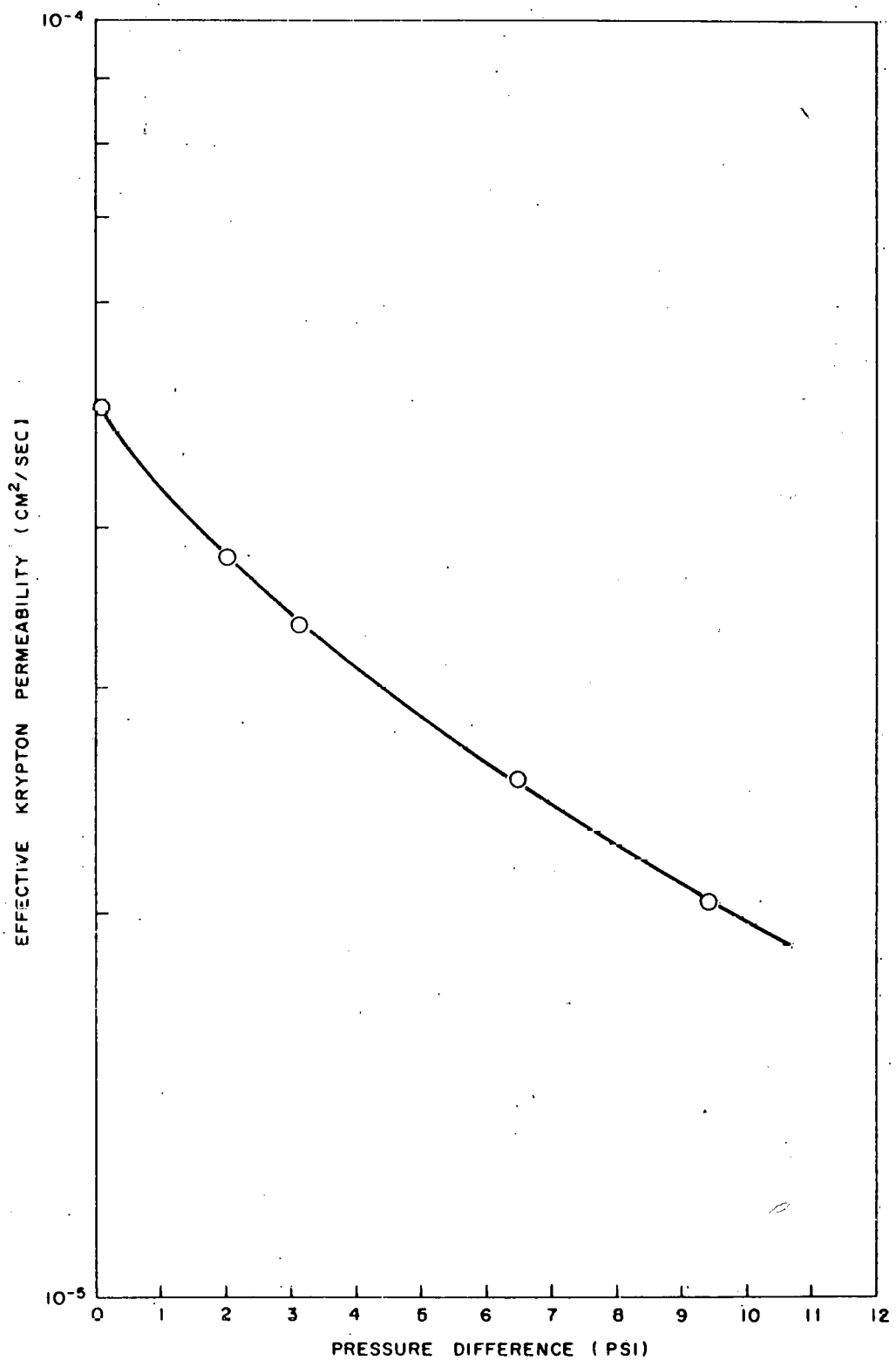

Fig. 6.10--Effective back-diffusion coefficient for krypton versus pressure difference (NCD3 graphite)

Several tests were conducted to determine if HTGR fuel-handling equipment could be decontaminated effectively should such equipment be grease-lubricated. A gear mechanism was lubricated with a tacky, viscous, radiation-resistant grease (Mobil XTR-23). Immersion of the mechanism in a highly basic solution heated to 250°F removed up to 99% of the grease in 15 to 25 min. This solution was the most effective of the general decontaminants tested.

Internal Trap Studies

Visual examination of the internal-trap reagent (Barnebey-Cheney Ag-coated carbon) from element III-A revealed no reagent damage. Adherence of the 15 wt-% silver coating is apparently good under in-pile-loop conditions.

Studies have been made on acceptance tests for internal-trap reagents to be used in the Peach Bottom reactor. An iodine dynamic sorption (breakthrough) test appears to be satisfactory.

THIS PAGE

WAS INTENTIONALLY

LEFT BLANK

TASK VIII. OVER-ALL PLANT ANALYSIS

8.1. SAFETY ANALYSIS AND HAZARDS

Turbine-generator Coastdown

Revised calculations were made of turbine-generator coastdown after turbine trip and loss of outside power. The essential electrical load was revised, which is the basic difference from the previous calculation.

Helium Blowdown

Revised recalculations were made of the blowdown of helium following ruptures at various locations in the primary coolant system, taking into account the present design, pressures and temperatures. In no credible case did levitation of the core result.

Fission-product Boiloff

A Fortran code, RETAIN, has been written to recalculate the retention of neutron poison material and fission products in the core, as well as their condensation and revaporization from the upper reflector following a complete loss-of-coolant-circulation accident. The RETAIN code utilizes the revised RAT digital calculations of temperatures versus time following this accident, and the end-of-life isotopic-fission-product densities provided by the FEVER code.

THIS PAGE

WAS INTENTIONALLY

LEFT BLANK

Appendix I

GENERAL ATOMIC REPORTS ISSUED ON THE HTGR PROJECT FROM APRIL 1, 1962, THROUGH JUNE 30, 1962

FORMAL REPORTS

GA-2630 CARBON TRANSPORT AND CORROSION IN HIGH-TEMPERATURE GAS-COOLED REACTORS, L. R. Zumwalt, R. D. Burnette, and A. B. Riedinger, April 12, 1962.

GA-2827 DEVELOPMENT AND EVALUATION OF B_4C-GRAPHITE CONTROL-ROD MATERIALS FOR THE HTGR, W. V. Goeddel, April 14, 1962.

GA-2998 EXPOSURE OF REACTOR STRUCTURAL MATERIALS TO IMPURE HELIUM AT ELEVATED TEMPERATURES, A. F. Weinberg and J. M. Scoffin, March 22, 1962.

GA-3041 PERFORMANCE OF A GAS-BEARING COMPRESSOR IN THE GENERAL ATOMIC HTGR IN-PILE LOOP, R. Stella, March 28, 1962.

GA-3064 BORON CARBIDE–GRAPHITE NUCLEAR CONTROL-ROD MATERIAL: PREPARATION, THERMAL STABILITY, AND IRRADIATION EVALUATION, Walter V. Goeddel, Harold K. Lonsdale, and Robert A. Meyer, April 24, 1962.

GA-3067 EVALUATION OF (Th, U)C_2, CARBON-COATED (Th, U)C_2 PARTICLES, AND CARBON COATINGS, G. B. Engle, C. S. Luby, and J. C. Bokros, April 26, 1962.

GA-3211 STEADY-STATE RELEASE FRACTION OF KRYPTON AND XENON FISSION PRODUCTS AT HIGH TEMPERATURES FROM (U, Th)C_2–GRAPHITE FUEL MATRIX IN OUT-OF-PILE EXPERIMENTS, E. E. Anderson, P. E. Gethard, and L. R. Zumwalt, June 15, 1962.

INFORMAL REPORTS

AMD-657 EROSION OF GRAPHITE BY HELIUM RECOILS FROM NEUTRON SCATTERING AND BY FORMATION OF HeC, E. Creutz and S. Cunningham, January 22, 1959.

GAMD-680 THE CALCULATIONS OF MONATOMIC GAS SCATTERING KERNELS, J. Gauer, February 17, 1959.

GAMD-925 TWO WOLONTIS PROGRAMS USEFUL IN REACTOR KINETICS STUDIES, R. Engelmore, August 10, 1959.

GAMD-1172 ANALYSIS OF STRESSES IN THE CENTRAL PORTION OF MONEL-CLAD FUEL ELEMENTS DURING THERMAL CYCLING, G. Donaldson, December 18, 1959.

GAMD-1233 VAPOR TRANSPORT OF URANIUM FROM UC_2-C COMPACTS, D. V. Ragone and L. R. Zumwalt, February 5, 1960.

GAMD-1318 KINEMATIC AND DYNAMIC ANALYSIS OF RADIAL ARM INDEXING MECHANISM TOP TRANSFER MACHINE, D. Nicoll and M. E. Timin, March 24, 1960.

GAMD-1375 DESIGN CRITERION OF PLENUM TO REFLECTOR BLOCK SEAL FOR HTGR REACTOR VESSEL, W. A. Kalk, April 20, 1960.

GAMD-1558 ANALYSIS OF A HOT SPOT IN THE PRESSURE VESSEL WALL, H. F. Menzel, July 28, 1960.

GAMD-1895 ANALYSIS OF VARIOUS METHODS OF HOLDING THE HTGR CORE, F. B. Nimtz, December 19, 1960.

GAMD-2221 PROCEDURES FOR THE PREPARATION OF GRAPHITE-MATRIX FUEL COMPACTS CONTAINING CARBON-COATED (Th, U)C_2 FUEL PARTICLES, W. V. Goeddel, April 27, 1961.

GAMD-2408 SIGMA-GAS 7090 VERSION, J. Bell, July 17, 1961.

GAMD-2660 CRITICAL REVIEW OF THE METHODS FOR TREATING GEOMETRIC EFFECTS IN HTGR ANNULAR RESONANCE INTEGRAL CALCULATIONS, J. B. Sampson, November 29, 1961.

GAMD-2675 THERMAL STABILITY TESTING OF GRAPHITE-MATRIX FUEL COMPACTS CONTAINING PYROLYTIC-CARBON-COATED CARBIDE PARTICLES WITH COMMENTS ON THE "AMOEBA" EFFECT, W. V. Goeddel, September 26, 1961.

GAMD-2885 "CTTS" CHANNEL TRAP TAPE SELECT, William A. Growdon, January 23, 1962.

Appendix II

PROJECT PERSONNEL

The research and development program on the prototype HTGR is being carried out by the following:

Assistant Director of the Laboratory	Duffield, R. B.
Project Manager	Born, M. R.
Administrative Assistant	Ledbetter, R. J.
HTGR Reporting	Hill, E. L.
Planning and Scheduling	Habush, A. L.
Reactor Section	
Fuel-handling Equipment	Nicoll, D. Hedgecock, J.
Control Rod and Control-rod Drive	Ledin, E.
Flow-model Data Reduction	Ross, S. (Public Service Company of Colorado)
Fuel Element Design	Turner, R. F. Vanslager, F. E.
Engineering Analysis Section	Rockenhauser, W. Hinz, P. F. Hunt, P. S. Menzel, H. F. Shao, L. C.
Chemistry Section	Zumwalt, L. R. Anderson, E. Burnette, R. D. Busch, D. D. Gethard, P. E. Lonsdale, H. Riedinger, A. B. Graves, G. C. Hancock, C. A. Milstead, C. E.

Hazards Analysis	Moffette, T. R. Landoni, J. A.
Physics Section	Stewart, H. B. Fischer, P. U. Merrill, M. H. Van Howe, K. R. Sampson, J. B. Nordheim, L. W. (part time) Bingham, B. A. Lane, R. K.
Metallurgy	Wallace, W. P. Engle, G. B. Goeddel, W. V.
Experimental Operations and Operations Analysis	
Operating Procedures	Paget, J. A. Delaney, G. W. (Central Illinois Public Service) Gibbons, J. P. (Philadelphia Electric Co.) Kemper, J. S. (Philadelphia Electric Co.) Logue, R. H. (Philadelphia Electric Co.)
In-pile-loop Experiments	Godsin, W. W. Baumgartel, R. Lofing, D. Cytron, S.
Capsule Irradiation	Sleigh, J. H., Jr.
Drafting and Graphic Arts	Albright, P. C. Dorion, G. O. Knell, S. W. Ringsmuth, R. J.